HHS Public Access

Author manuscript

Nat Cell Biol. Author manuscript; available in PMC 2019 September 25.

Published in final edited form as:

Nat Cell Biol. 2017 August ; 19(8): 974–987. doi:10.1038/ncb3578.

Obesity alters the lung myeloid cell landscape to enhance breast cancer metastasis through IL5 and GM-CSF

Daniela F. Quail[1,7], **Oakley C. Olson**[1,7], **Priya Bhardwaj**[2], **Logan A. Walsh**[3], **Leila Akkari**[1,4,5], **Marsha L. Quick**[1], **I-Chun Chen**[2], **Nils Wendel**[2], **Nir Ben-Chetrit**[1,2], **Jeanne Walker**[6], **Peter R. Holt**[6], **Andrew J. Dannenberg**[2], **Johanna A. Joyce**[1,4,5,8]

[1]Cancer Biology and Genetics Program, Memorial Sloan Kettering Cancer Center, New York, New York 10065, USA [2]Department of Medicine, Weill Cornell Medical College, New York, New York 10065, USA [3]Human Oncology and Pathogenesis Program, Memorial Sloan Kettering Cancer Center, New York, New York 10065, USA [4]Ludwig Institute for Cancer Research, Lausanne 1066, Switzerland [5]Department of Oncology, University of Lausanne, Lausanne 1066, Switzerland [6]Laboratory of Biochemical Genetics and Metabolism, The Rockefeller University, New York, New York 10065, USA [7]These authors contributed equally to this work.

Abstract

Obesity is associated with chronic, low-grade inflammation, which can disrupt homeostasis within tissue microenvironments. Given the correlation between obesity and relative risk of death from cancer, we investigated whether obesity-associated inflammation promotes metastatic progression. We demonstrate that obesity causes lung neutrophilia in otherwise normal mice, which is further exacerbated by the presence of a primary tumour. The increase in lung neutrophils translates to increased breast cancer metastasis to this site, in a GM-CSF- and IL5-dependent manner. Importantly, weight loss is sufficient to reverse this effect, and reduce serum levels of GM-CSF and IL5 in both mouse models and humans. Our data indicate that special consideration of the obese patient population is critical for effective management of cancer progression.

Tumours develop in complex microenvironments containing diverse cell types and inflammatory mediators[1,2]. Beyond the local tumour microenvironment, an inflammatory systemic environment can also affect disease outcome, by perturbing homeostasis within multiple tissues throughout the body[3]. This becomes particularly important during metastasis, where systemic alterations can modify the tissue landscape of distant organs and support tumour cell colonization by establishing a pre-metastatic niche[4]. Indeed, chronic

[8]Correspondence should be addressed to J.A.J. (johanna@joycelab.org).

AUTHOR CONTRIBUTIONS

D.F.Q., O.C.O. and J.A.J. conceived the study, designed and interpreted experiments, and wrote the manuscript. D.F.Q., O.C.O., P.B., L.A.W., L.A., M.L.Q., I.-C.C., N.W. and N.B.-C. performed experiments and analysed results. J.W., P.R.H. and A.J.D. provided human sera and blood, and A.J.D. helped design and interpret experiments. J.A.J. supervised the study. All authors commented on the manuscript.

Note: Supplementary Information is available in the online version of the paper

COMPETING FINANCIAL INTERESTS

The authors declare no competing financial interests.

inflammation can increase cancer risk and/or progression[5]. Investigation into how the systemic environment affects tumour biology is therefore critical for an integrated understanding of cancer[3].

A prevalent and clinically relevant example of systemic inflammation is obesity, which affects >30% of adults in the US, and is linked to multiple pathologies, including cancer[6]. As a growing epidemic, obesity now rivals smoking as the leading preventable cause of cancer[7]. Obesity-associated inflammation is driven in part by adipocyte-myeloid cell interactions within various fat depots, resulting in altered immune cell composition in different tissues[8–12]. Thus, an emerging hypothesis is that obesity-associated inflammation promotes cancer progression[11], aligning with well-established associations between other chronic inflammatory conditions and tumorigenesis[13].

Clinical analyses have shown that obesity is associated with higher incidence of breast cancer metastasis[14], particularly to liver and lung[15]. However, insight into the mechanisms underlying obesity-induced metastasis, compared with the effects on primary tumour growth[16], has been limited. Of particular interest is lung metastasis, given the high frequency of breast cancer dissemination to this site in patients[17], and the strong clinical association between obesity and multiple lung-inflammatory conditions[18,19], despite the lack of adipose tissue within the lung. Therefore, we sought to analyse the effects of obesity-associated inflammation on breast-to-lung metastasis using animal models, focusing on myeloid cell populations given their role during adipose inflammation[20] and pulmonary metastasis in non-obese settings[21–29].

RESULTS

Obesity is associated with lung neutrophilia driven by high adiposity

To investigate the effects of obesity on lung inflammation, we used a diet-induced obesity (DIO) model; wild-type (WT) C57 black6 (BL6) female mice were enrolled on either a low-fat (LF; 10% kcal) or high-fat (HF; 60% kcal) diet for 15 weeks followed by immunoprofiling. We found HF lungs exhibited elevated proportions of $CD45^+$ leukocytes (~ 13–19% of total cells), $CD11b^+Gr1^-$ macrophages (~3–4% of total cells) and $CD11b^+Gr1^+$ myeloid cells (~2–7% of total cells) by flow cytometry (Fig. 1a,b and Supplementary Table 1). The increase in $CD11b^+Gr1^+$ cells was confirmed with antibodies independently targeting Ly6C and Ly6G ($CD11b^+Ly6C^{lo}Ly6G^+$; Fig. 1b and Supplementary Fig. 1a). Cytospin and Giemsa staining identified $CD11b^+Gr1^+$ cells as predominantly hyper-segmented neutrophils (Supplementary Fig. 1b). Of note, we observed no changes in the proportions of bulk T lymphocytes (total $CD3^+$ cells; ~8–9% of total cells) or T-cell subsets ($CD3^+CD4^+$, ~2–3% of total cells; $CD3^+CD8^+$, ~1–2% of total cells) in HF lungs (Supplementary Fig. 1c).

To uncouple whether this increase in lung neutrophils was due to high adiposity or diet content, we first analysed the *ob/ob* genetic model of obesity[30], in which animals fed a normal diet exhibit rapid weight gain (Fig. 1c) due to hyperphagia secondary to leptin deficiency *Ob/ob* lungs exhibited elevated proportions of neutrophils by flow cytometry, but no significant changes in overall leukocytes or macrophages (Fig. 1d). In a reciprocal

experiment, we employed a BALB/c model of obesity resistance, whereby WT BALB/c mice were fed HF or LF diet for 15 weeks, but did not gain weight (Fig. 1e). Unlike most other mouse strains, this obesity-resistance phenotype is inherent to BALB/c animals[31]. We found no significant increase in neutrophils (Fig. 1f), in contrast to results from DIO and *ob/ob* mice. These data suggest that the increase in lung neutrophils is due to high adiposity of obese animals, rather than diet/nutrient content.

We next profiled other common organs for breast cancer dissemination, including liver and brain. DIO mice exhibited no change in immune cell proportions in brain, including macrophages and neutrophils (Supplementary Fig. 1d and Supplementary Table 1). While we detected a significant increase in neutrophil proportions in the liver, these differences were inversely correlated with the *ob/ob* model (Supplementary Fig. 1e), suggesting that the changes in this organ may be diet-dependent, unlike our findings in the lung (Fig. 1d). We therefore focused subsequent experiments on the effects of adiposity on lung inflammation, and neutrophils specifically, as this was the only immune cell population consistently elevated in the lung across the different obesity models.

We next asked whether obesity-associated lung neutrophilia was reversible. Animals were enrolled on HF diet for 15 weeks, and switched to LF for an additional 7 weeks (Supplementary Fig. 1f). Mice lost an average of 28% of their body weight over the diet-switch period (Fig. 1g). Lung neutrophils decreased after diet-switching, compared with animals that remained on continuous HF diet (Fig. 1h), indicating that obesity-associated lung neutrophilia is reversible with weight loss.

Obesity-associated lung neutrophilia is accompanied by pro-metastatic gene expression changes and enhanced metastatic progression

It is known that neutrophils, defined as either $CD11b^{+}Gr1^{+/hi}$ or $CD11b^{+}Ly6G^{+}$ by flow cytometry, are elevated in the pre-metastatic lung in PyMT breast cancer models, and become activated to support metastatic progression[24,25,27,29]. We therefore asked whether lung neutrophils were activated in obese mice, and how this might affect breast cancer metastasis. We purified lung neutrophils from LF and HF animals (DIO model) using fluorescence-activated cell sorting (FACS), and performed quantitative PCR with reverse transcription (qRT-PCR) for a panel of markers relevant to neutrophil biology in cancer[32]. We focused on genes related to mobilization (*Cxcl2, Cxcl12, Cxcr4, Cxcr2* and *Tlr4*[33–35]), 'N2-like' polarization (*Arg1, Ccl5, Ccl2* and *Tgfb1*[36,37]), immune suppression (*Il10, Nox2, Nos2, Pge2, Ptgs2* and *Pdl1*[38–40]) and activation/expansion (*Il1b* and *Nlrp3*[41], *Alox5*[24], *S100A9* and *S100A8*[42]). Markers of N2-like polarization were significantly downregulated in HF neutrophils (Fig. 2a), suggesting discordance with the 'N1/N2-like' paradigm[36]. We observed significant increases in several markers associated with mobilization (3/3 upregulated) and activation (4/5 upregulated), and variable changes in markers associated with immune suppression (2/6 upregulated and 1/6 downregulated; Fig. 2a), indicating that HF neutrophils were phenotypically different from LF neutrophils, in addition to being more abundant. Interestingly, many gene expression changes in association with obesity were indicative of a pro-metastatic phenotype, for example, *Alox5, S100a8/9* and *Cxcr2/4*[25,33,34,42].

We next investigated whether the elevation in neutrophil number/activation during obesity was associated with enhanced lung metastasis. We generated a syngeneic immune-competent breast cancer model compatible with the BL6 DIO model, by isolating a panel of cell lines from BL6 MMTV-PyMT mice and confirming that they form orthotopic tumours that spontaneously metastasize to lung after ~2 months (Supplementary Fig. 2a–d). Orthotopic transplantation of two of these lines (99LN, 86R2) into the DIO model revealed that primary tumour growth was modestly enhanced with HF feeding over a 2-month period (Fig. 2b and Supplementary Fig. 2e). Systemic neutrophilia was monitored at different time points: prior to tumour cell injection (0 d), when tumours were palpable (14 d), during early phases of primary tumour growth (28 d; pre-metastatic niche) and late phases of primary tumour growth (56 d; micro-metastatic disease). At 0 d, circulating neutrophils were elevated in HF versus LF mice, and as primary tumours grew, a significant difference in neutrophilia was maintained (Fig. 2c). At early phases of primary tumour growth (28 d), we quantified neutrophils in the pre-metastatic lung, and found that while lean tumour-bearing mice exhibited lung neutrophilia compared with lean non-tumour-bearing mice (as has been reported[24,25,27,29,37,43,44]), obesity significantly enhanced neutrophilia in the tumour-bearing setting (Fig. 2d). At the trial endpoint (56 d), we found elevated micro-metastases in the lung (Fig. 2e and Supplementary Fig. 2f), concomitant with increased lung neutrophilia in obese compared with lean mice (Fig. 2d). These data indicate that obesity enhances spontaneous lung metastasis, and contributes to lung neutrophilia in a manner that is additive to pre-metastatic niche observations obtained in standard (lean) mouse models.

Obesity enhances experimental breast cancer metastasis to lung in a neutrophil-dependent manner

Given the differences in primary tumour volumes between HF and LF mice, we investigated whether obesity affects experimental metastasis of breast cancer cells via tail vein injection. We labelled 99LN cells with luciferase-GFP, to allow for bioluminescent imaging (BLI) and flow cytometry, and monitored experimental lung metastasis over 5 weeks. HF mice exhibited significantly higher luminescence in the lung compared with LF mice after 5 weeks (Fig. 3a,b), which was confirmed by flow cytometry for GFP^+ tumour cells (Fig. 3c). Moreover, we found that the increased proportion of neutrophils during obesity was also evident in the tumour-bearing setting (Fig. 3d).

Given the roles of neutrophils in establishing a pre-metastatic niche[25,27,29] and influencing early seeding[24,43], we examined the effects of obesity on earlier metastatic time points[45]. We analysed lung metastasis 48 h following tail vein injection of 99LN cells into the DIO model. HF mice exhibited significantly higher luminescence in the lung compared with LF mice (Fig. 3e), consistent with flow cytometry of GFP^+ tumour cells (Fig. 3f). Immunoprofiling of lung showed that obesity-induced neutrophilia was evident in this early metastatic setting (Fig. 3g). Similar observations were made for experimental metastasis in the *ob/ob* model (Supplementary Fig. 3a,b), where expression analysis revealed an upregulation of pro-metastatic genes in *ob/ob* lung neutrophils compared with WT (Supplementary Fig. 3c).

Given the short duration of the 48 h experimental metastasis model, we suspected that neutrophils affect pro-metastatic processes beyond suppression of the adaptive immune response, as is frequently reported for $CD11b^+$ $Gr1^+$ myeloid-derived suppressor cells[25,27,32]. In co-culture experiments, HF neutrophils did not exhibit an enhanced capacity to modulate cytotoxic T-cell proliferation or NK cell degranulation *in vitro* (Supplementary Fig. 3d–f), nor did we observe enhanced NK cell suppression *in vivo* (Supplementary Fig. 3g). These findings suggest that HF neutrophils are not immunosuppressive, unlike their myeloid-derived suppressor cell counterparts, and affect early metastatic seeding; therefore, we restricted further analyses to the 48 h metastasis model.

Next, we assessed whether neutrophils were functionally important during obesity-associated lung metastasis. We used a neutralization antibody against Gr1 (clone RB6–8C5[9]), and confirmed treatment efficacy in blood, lung and spleen (Supplementary Fig. 4a–c). Using the 48 h experimental metastasis assay, we found that Gr1 neutralization in HF mice significantly reduced lung metastasis compared with IgG controls, confirmed by BLI and flow cytometry (Fig. 3h,i). These data demonstrate that obesity-associated lung neutrophilia supports subsequent metastatic seeding.

Elevated GM-CSF in serum underlies obesity-associated lung neutrophilia and breast cancer metastasis

We next asked how lung neutrophil numbers are elevated during obesity. Blood analyses of LF and HF animals revealed enhanced neutrophilic leukocytosis associated with HF feeding (Fig. 4a), consistent with reported findings from human subjects with high body mass index (BMI)[46], and with the orthotopic trial results (Fig. 2c). We hypothesized that circulating factors may contribute to regulating this systemic inflammatory phenotype, and collected serum from LF and HF mice for *in vitro* myelopoiesis assays. Intriguingly, HF serum supported differentiation of bone marrow (BM) towards a CD11b+Gr1+ phenotype more effectively than LF serum (Fig. 4b). Critically, we confirmed this result with serum from obese and lean human donors (Fig. 4c).

To identify serum factors supporting myelopoiesis, we performed a cross-species cytokine screen of 103 factors, using serum from both mice and humans (Supplementary Table 2). Thirty factors were enriched in mouse HF serum compared with LF serum, and 16 factors were enriched in human obese serum compared with lean serum. Of these, 8 were upregulated in both species, including CCL25, CD40L, GM-CSF, IGFBP2, IL5, IL6, MMP3 and MMP9 (Fig. 4d and Supplementary Fig. 5a–d). Using recombinant proteins in the *in vitro* myelopoiesis assay, we found that only GM-CSF was capable of enhancing differentiation towards a $CD11b^+Gr1^+$ phenotype (Fig. 4e). Antibody-mediated neutralization of GM-CSF in the context of HF serum reduced $CD11b^+Gr1^+$ differentiation *in vitro*, to a level comparable to LF serum (Fig. 4f), demonstrating the necessity of this factor.

Intriguingly, analysis of GM-CSF (*Csf2*) expression by qRT-PCR of bulk tissues from obese mice revealed a marked enrichment in whole lung compared with spleen, blood, BM, liver and fat (Fig. 4g and Supplementary Fig. 5e–k). This is consistent with *Csf2* mouse knockout studies demonstrating a tissue-specific role for GM-CSF in lung physiology and

inflammation[47–49]. Moreover, in FACS-purified cell populations from obese lungs, *Csf2* was expressed by multiple immune cell types including various myeloid cells (for example, Ly6C^{hi} monocytes), and CD3^{+} bulk T cells (Fig. 4h), suggesting that maintenance of neutrophils in the lung is due to both autocrine signalling and paracrine interactions with additional immune cell populations. These data implicate GM-CSF as a regulator of lung neutrophilia in the context of obesity.

To test whether GM-CSF alone was capable of recapitulating obesity-induced lung neutrophilia *in vivo*, we treated WT animals with recombinant (r) GM-CSF for 5 d, followed by flow cytometry analysis. Even after this short time period, there was a significant increase in the proportion of neutrophils in blood and lungs in response to rGM-CSF compared with controls (Fig. 5a). This result is consistent with previous reports showing that GM-CSF regulates lung neutrophilia in models of pulmonary alveolar proteinosis, asthma, bronchitis and pulmonary infection[18,48–50]. Significant differences in neutrophil numbers within immune reservoirs such as the spleen or BM were not observed during this short experimental time course (Supplementary Fig. 6a,b), suggesting that this change was not driven by neutrophil expansion within those depots.

We next asked whether GM-CSF was sufficient to modulate metastatic outcome *in vivo*. We treated WT animals on a normal diet with rGM-CSF for 5 d to induce neutrophilia (Fig. 5a), followed by a 48 h experimental metastasis assay using 99LN breast cancer cells injected intravenously (Fig. 5b). We observed a significant increase in metastases, as measured by BLI in the lung at 48 h, in animals treated with rGM-CSF compared with PBS controls (Fig. 5c). In a reciprocal experiment, we enrolled animals on either a HF or LF diet for 15 weeks, followed by antibody-mediated neutralization of GM-CSF prior to injecting 99LN cells intravenously (Fig. 5d). At the trial endpoint of 48 h we found that GM-CSF neutralization in HF-fed animals, but not LF animals, resulted in a significant decrease in lung BLI compared with IgG control (Fig. 5e), corroborating our Gr1-neutralization results (Fig. 3h,i). These results were validated by flow cytometry of GFP^{+} tumour cells in lung (Fig. 5f). Importantly, when we immunoprofiled the lungs, we found that the proportion of neutrophils was significantly reduced in HF animals after GM-CSF neutralization compared with IgG, but this effect was not observed for LF animals (Fig. 5g). Together, these results demonstrate that obesity-associated GM-CSF is critical to support lung neutrophilia and enhanced metastatic seeding.

We then asked whether serum GM-CSF was elevated in response to a primary tumour, as reported for the related factor G-CSF[25,27,29]. Enzyme-linked immunosorbent assay (ELISA) for GM-CSF in serum isolated from the orthotopic experiments showed a modest (non-significant) increase in GM-CSF in lean mice in response to the presence of a primary tumour; this effect was significantly increased with obesity, and even more pronounced during later stages of progression (Fig. 5h). These data indicate that obesity may exacerbate the stimulatory effects of a primary tumour on neutrophils.

IL5 signalling supports obesity-associated lung neutrophilia

We next explored how obesity induces GM-CSF expression. From our findings in *ob/ob* and Balb/c mice (Fig. 1c–f), we determined that adiposity was an important contributor to lung

neutrophilia. Therefore, we investigated which of the 8 upregulated factors from the cytokine array (Fig. 4d) were specifically enriched in adipose tissue. We found that *Il5* expression was enriched in both subcutaneous and visceral fat in obese animals (Fig. 6a), and highest in adipose tissue compared with spleen, blood, BM, liver and lung (Supplementary Fig. 5e). IL5 plays a canonical role in regulating eosinophils, another type of granulocyte, during allergic asthma[19,51]. Given the link between obesity and adult-onset asthma[19], we wanted to determine the relevance of IL5 to neutrophil regulation. In WT animals, treatment with rIL5 for 5 d significantly increased the proportion of lung neutrophils compared with PBS controls (Fig. 6b,c). $CD3^+$ T cells, another GM-CSF-producing cell population in the lung (Fig. 4h), were also elevated in response to rIL5 (Supplementary Fig. 7a). Furthermore, increased neutrophils led to enhanced experimental lung metastasis, which was blocked by GM-CSF neutralization (Supplementary Fig. 7b–d). These data suggest that neutrophils are in part regulated by IL5, either by direct or indirect mechanisms.

We next determined which cell types respond directly to IL5, by identifying populations that express the IL5 receptor. The IL5 receptor has an alpha-subunit (IL5rα) and beta-subunit (Csf2rβ). Interestingly, the beta-subunit is shared between IL5, GM-CSF and IL3; a reflection of their complementary roles during airway inflammation and Th2 immunity in asthma[52]. Csf2rβ is broadly expressed on myeloid cells, and induces signal transduction in response to IL5, while IL5rα expression is more limited and dictates cellular specificity of IL5 signalling. Most of the literature on IL5r*α up* is focused on expression by eosinophils (reviewed in ref. 53), with only a few studies reporting eosinophil-independent effects of IL5[54–56]. However, by flow cytometry we determined that 99% of neutrophils and 68% of monocytes isolated from HF peripheral blood express IL5rα, as compared with $CD11b^+SSC^{hi}SiglecF^+$ eosinophils, which were 100% positive for IL5rα as expected (Fig. 6d). When we quantified *Csf2ra, Csf2rb* and *Il5ra* expression in FACS-purified $IL5r\alpha^+$ lung neutrophils, eosinophils and monocytes from the DIO model, we found that in several instances, the genes encoding these receptor subunits were upregulated by obesity (Fig. 6e). This is consistent with reports of upregulated *Il5ra* in neutrophils and monocytes in response to sepsis-associated inflammation[54], and methylation analyses that predicted *IL5RA* upregulation in circulating immune cells in response to obesity in humans[57]. Corroborating these results, by flow cytometry we found a subset of $IL5R\alpha^+$ intermediate monocytes from human blood (mean = 23.4% positive), as well as a smaller proportion of neutrophils (mean = 12.2% positive), classical monocytes (mean = 12.3% positive), and non-classical monocytes (mean = 11.8% positive) when eosinophils were used as a positive gating control (Fig. 6f).

We were unable to detect *Il5ra* expression by qRT-PCR on $CD3^+$ T cells isolated from lungs in the DIO model. However, given our findings that $CD3^+$ T cells isolated from obese lung tissue express *Csf2* (Fig. 4h), and the increase in $CD3^+$ T-cell numbers in the lung following rIL5 treatment *in vivo* (Supplementary Fig. 7a), we wanted to directly test whether T cells were important for IL5-mediated lung neutrophilia. We treated athymic nude mice with rIL5 for 5 d, and found that lung neutrophilia in response to IL5 treatment did not occur in the absence of T cells (Supplementary Fig. 7e). In addition, the proportion of $IL5r\alpha^+$ myeloid cells in nude mice was significantly reduced compared with BL6 mice (monocytes reduced

from 68% to <1%; neutrophils 99% to 9%; eosinophils 100% to 90%; Supplementary Fig. 7f). Similar results were observed in NOD-*scid Il2rg*^{null} (NSG) mice, which lack mature T, B and NK cells (Supplementary Fig. 7e,f). Taken together, our findings indicate that T cells are indispensable for IL5-induced lung neutrophilia.

We next asked which IL5rα$^+$ cell type was capable of mediating a functional response to IL5. We FACS-purified IL5rα$^+$ cells from the peripheral blood of BL6 mice, including monocytes, neutrophils and eosinophils, and treated them *in vitro* with rIL5. Not surprisingly, by flow cytometry we observed increased Ki67$^+$ proliferating IL5rα$^+$ eosinophils in response to rIL5 (Fig. 6g)—a canonical effect of IL5 in this cell type. We also found increased proliferation of IL5rα$^+$ monocytes in response to rIL5 *in vitro* (Fig. 6g), concomitant with upregulated *Csf2* expression by qRT–PCR (Fig. 6h). In the DIO model, we confirmed that obesity increases IL5rα$^+$ monocyte abundance in blood and lung, concomitant with an increase in *Csf2* expression, compared with LF controls (Fig. 6i,j). These data indicate that IL5rα$^+$ monocytes directly respond to IL5 by expanding in numbers and producing GM-CSF, and may thereby contribute to lung neutrophilia during obesity.

Obesity enhances lung homing of neutrophils in an IL5-dependent manner

Given that HF lung neutrophils upregulate genes associated with mobilization (Fig. 2a), such as *Tlr4, Cxcr2* and *Cxcr4*[33–35], we asked whether obesity alters homing and/or retention of neutrophils in the lung, and whether this is dependent on IL5. We isolated and fluorescently labelled neutrophils from BM of WT (green) and *ob/ob* (red) donors, mixed them 1:1, and performed adoptive cell transfer back into WT, *ob/ob* or *ob/ob* + anti-IL5 recipients (Fig. 7a,b). We found that 4h post-adoptive transfer, the majority of labelled neutrophils in the lung across all recipient groups were from *ob/ob* donors (Fig. 7c,d), despite equivalent proportions of WT and *ob/ob* neutrophils in blood (Fig. 7e), indicating that neutrophils from obese animals are predisposed to lung homing. Furthermore, lung trafficking of *ob/ob* donor neutrophils was significantly enhanced in *ob/ob* recipients compared with WT recipients, and this effect was mitigated by IL5 neutralization (Fig. 7c). This suggests that obesity primes the lung microenvironment to support neutrophil homing in an IL5-dependent manner. After 8 h, neutrophil clearance within the lungs and blood was comparable between donor groups (Supplementary Fig. 8a,b); however, *ob/ob* recipient animals retained the highest levels of lung neutrophils regardless of donor genotype (Fig. 7f,g). Interestingly, this capacity for neutrophil retention was blocked by IL5 neutralization (Fig. 7f,g). These data indicate that obesity supports increased lung homing and retention of neutrophils in an IL5-dependent manner.

Weight loss reduces obesity-associated lung neutrophilia and metastasis

Given our observation that diet-switch reverses obesity-induced lung neutrophilia in the DIO model (Fig. 1g,h), and the relevance of this non-invasive intervention strategy to patients, we investigated whether weight loss could similarly reduce obesity-associated metastasis. We confirmed that IL5rα$^+$ neutrophils and monocytes were upregulated in HF lungs, which was reversed by diet-switching (Fig. 8a–c). We found that diet-switching reversed experimental lung metastasis (Fig. 8d), and the expression of key markers of neutrophil activation/mobilization, including *Cxcr2* and *S100A8* (Fig. 8e). Finally, serum analysis by ELISA

showed reduced GM-CSF and IL5 in diet-switched mice, compared with mice fed continuous HF diet (Fig. 8f). These data indicate that diet changes in association with weight loss may be sufficient to reverse the pro-metastatic effects of obesity.

Finally, we asked whether weight loss intervention was sufficient to reduce key serum factors identified here (that is, GM-CSF, IL5) in a human clinical trial. We obtained matched serum samples from 10 female obese humans before and after 10% weight loss by caloric restriction[58] (ClinicalTrials.gov Identifier:). Consistent with results from the DIO model, there was a significant decrease in circulating neutrophils with weight loss[58], corroborating observations of reduced leukocytosis following bariatric surgery in obese humans[59]. Following assessment of serum levels of GM-CSF and IL5 in matched individuals, we found that these factors were generally reduced following weight loss (Fig. 8g), Similarly, weight loss resulting from surgical intervention has been shown to reduce serum levels of GM-CSF and IL5 in accordance with a reduction in BMI[60]. These results demonstrate the potential translational relevance of our findings to humans, and indicate that weight loss interventions may be useful to improve outcomes in obese breast cancer patients.

DISCUSSION

In this study, we have identified lung neutrophilia as a secondary effect of obesity. This occurs independently of diet; rather it is directly related to increased adiposity and the expression of IL5 by adipose tissue. IL5 has been reported as a negative regulator of adipose tissue expansion and insulin resistance[61], thereby working to constrain the effects of obesity on metabolism. While in adipose tissue IL5 supports homeostasis[62], the increase in serum IL5 has the opposite effect on lung. We found that IL5 increases *Csf2* expression by IL5rα$^+$ monocytes, and neutrophil trafficking to lung. Furthermore, increased serum GM-CSF promotes myelopoiesis, leading to an expansion of peripheral neutrophils (Fig. 8h). Collectively these findings demonstrate that obesity causes lung inflammation, despite the lack of adipose tissue in this organ, by acting through the systemic environment.

In tumour models, we showed that obesity-associated lung neutrophilia enhances breast cancer metastasis to this organ, and that depletion of Gr1$^+$ cells in obese animals reverses this effect. This is reminiscent of the pre-metastatic niche concept[4], although in this case the elevation of pro-metastatic neutrophils is observed in non-tumour-bearing animals, and exacerbated by the presence of a primary tumour Of particular interest was our observation that GM-CSF is predominantly expressed by lung in obese mice, and that GM-CSF blockade reverses the pro-metastatic effects of obesity. This suggests that disruption of normal lung homeostasis is a critical intermediary of obesity-induced metastasis, and that pharmacological interventions that resolve lung inflammation may reduce metastatic risk. However, neutrophil depletion is unlikely to be a safe option for patients. Alternatively, we have shown that targeting IL5 is sufficient to block lung neutrophil trafficking in obese mice; this strategy could be used to normalize the lung microenvironment without causing systemic neutropenia. Indeed, clinical evaluation of anti-IL5 therapy has confirmed the safety and efficacy of this approach in resolving eosinophilic asthma in patients, including the morbidly obese[63].

Our data suggest that obesity remains coupled to the pathological state of the lung, and that restoration of homeostasis within the adipose tissue through weight loss interventions will similarly normalize the lung microenvironment. In humans, we found that 10% weight loss in morbidly obese individuals was associated with reduced serum IL5 and GM-CSF, concomitant with decreased circulating neutrophils[58]. This is consistent with observations that caloric restriction reverses obesity-associated inflammation within mammary tissue[64], and enhances anti-tumour immunity[65]. Our findings also have implications for the long-term management of obese breast cancer patients, as pulmonary inflammation may have prognostic value. Monitoring serum levels of GM-CSF, IL5 or absolute neutrophil counts could prove useful to stratify the obese patient population, and identify those at highest risk of metastasis who may benefit from obesity-specific adjuvant therapies or dietary interventions. Clinical studies are therefore warranted to appropriately manage the obese cancer patient population, and uncouple the comorbidity of obesity and cancer.

While we have identified GM-CSF and IL5 as two critical cytokines that mediate obesity-enhanced lung metastasis in breast cancer, it is likely that additional factors are involved. Identifying drivers of the pro-metastatic phenotype of lung neutrophils in the context of high adiposity, and how the primary tumour influences these mechanisms, are important questions for future studies. Furthermore, it is unclear how an increase in circulating IL5 is achieved during obesity, and whether this affects other organs besides lung and adipose tissue. Given the importance of Th2 cytokines in promoting cancer progression in a primary tumour microenvironmen[1], a greater understanding of how IL5 affects breast cancer within adipose tissue of the obese mammary gland is warranted. Clinical translation of microenvironment-targeting agents has been hindered by patient heterogeneity and challenges in identifying individuals that will derive benefit. Investigating the effect of comorbidities, in this case obesity, on the microenvironment and cancer progression represents an important new direction in the field.

METHODS

Cell lines.

The MMTV-PyMT mouse model was backcrossed into the BL6 background for > 10 generations prior to isolating breast tumour cell lines. These cell lines were subsequently selected for their capacity to grow in the mammary fat pad (7×10^5 cells injected per mouse) of WT BL6 animals within a reasonable time period (<2 months). Three cell lines were selected for subsequent experiments, including 99LN, 86R2 and 91R2. All breast tumour cell lines in culture were maintained in DMEM supplemented with 10% FBS, and were validated to be mycoplasma-free. For assays involving immune cell culture, primary cells were isolated from peripheral sources (that is, blood or bone marrow) by FACS and used immediately for functional assays, for example NK cell co-culture or T cell CFSE, as described below.

Biological reagents and specifications.

Reagents for *in vitro* use were as follows: recombinant proteins (CCL25, CD40L, GM-CSF, IGFBP2, IL5, IL6, MMP3, MMP9, 100 ng ml^{-1} for all; R&D Systems); antibody-mediated

neutralization of GM-CSF (IgG versus anti-GM-CSF, 0.1 μg ml^{-1}; R&D Systems). Reagents for *in vivo* use were as follows: antibody-mediated neutralization of Gr1 (6μg g^{-1} body weight, dosed every 3 d intraperitoneally, clone RB6-8C5, rat IgG2b isotype control; Tonbo Biosciences)[9]; antibody-mediated neutralization of GM-CSF (16 μg g^{-1} bodyweight, dosed every 3 d intraperitoneally, clone MP122E9, rat IgG2a isotype control; R&D Systems)[66]; antibody-mediated neutralization of IL5 (1 mg kg^{-1} bodyweight, dosed 3 d and 1 d prior to adoptive cell transfer experiment intravenously, clone TRFK5, rat IgG1 isotype control; R&D Systems)[67]; recombinant mouse GM-CSF (50 μg kg^{-1} body weight, dosed every day for 5–7 d intraperitoneally, 2% BSA/PBS vehicle control; R&D Systems); recombinant mouse IL5 (8 μg kg^{-1} bodyweight, dosed every day for 5–7 d intraperitoneally, 2% BSA/PBS vehicle control; BD Pharmingen)[68].

Animal experiments.

All animal trials were approved by the Research Animal Resource Center (RARC) at MSKCC and the Institutional Animal Care and Use Committee (IACUC) and were performed in a manner compliant with all relevant ethical regulations regarding animal research. Details for specific animal models, including DIO, *ob/ob*, Balb/c and immune-compromised models, are described below.

Diet-induced obesity (DIO) model.

To model obesity with diet, 5-week-old female BL6 mice (Jackson Laboratory) were enrolled on either high-fat (HF; 60% kcal, Research Diets D12492) or low-fat (LF; 10% kcal, Research Diets D12450) irradiated rodent diet for 15 weeks. Weight was monitored over time. After 15 weeks, animals were either euthanized for flow cytometry, or injected with tumour cells (see 'Primary tumour growth assay' and 'Experimental metastasis assay' sections). For the diet-switch model (HF–LF), 5-week-old female BL6 mice were fed for 15 weeks with HF diet, and then switched to LF diet for 7 weeks[64] prior to euthanization.

Ob/ob model.

To control for the effects of adipose tissue content in mice, 4 week-old female B6.Cg-*Lep*^{ob} (*ob/ob*; Jackson Laboratory) mice were purchased and maintained on normal rodent diet. These mice gain weight due to a homozygous mutation in the leptin (*Lep*) gene that causes excessive eating and rapid weight gain. Weight was monitored over time beginning at 5 weeks old, and mice were euthanized when they reached >40g. This time period was significantly shorter (6 weeks) than that of the DIO model (15 weeks). After 6 weeks, animals were euthanized for flow cytometry analysis of myeloid cell populations in the lung, or injected with tumour cells for 48 h metastasis assays (see 'Experimental metastasis assay' section).

Balb/c obesity-resistant model.

To control for the effects of nutrient content in diet, 5 week-old WT Balb/c mice (Jackson Laboratory) were enrolled on either HF or LF diet (Research Diets, see 'DIO model') for 15 weeks. Balb/c animals do not gain weight in response to HF feeding[31]. After 15 weeks, animals were euthanized for flow cytometry analysis of myeloid cell populations in the lung.

Immune-compromised mouse models.

Two immune-compromised mouse models were used in this study, athymic nude (lack T cells) and NOD-*scid Il2rg*^{null} (NSG; lack mature T, B and NK cells). In both cases, 5-week-old female mice (Jackson Laboratory) were treated with recombinant mouse IL5 (8 μg kg^{-1} body weight, dosed intraperitoneally every day for 5 d, 2% BSA/PBS vehicle control; BD Pharmingen)[68], and flow cytometry was used to quantify lung neutrophils (CD45^{+}CD11b^{+}Ly6C^{lo}Ly6G^{+}), monocytes (CD45^{+}CD11b^{+}Ly6C^{hi}) and eosinophils (CD45^{+}CD11b^{+}SSC^{hi}Siglec-f^{+}).

Flow cytometry and fluorescence-activated cell sorting (FACS).

For flow cytometry of tissues, mice were anaesthetized with avertin, blood was collected by submandibular bleeding, and cardiac perfusion with PBS was performed. All tissues were mechanically dissociated and filtered through a 40 μm mesh to generate a single-cell suspension, and red blood cells were lysed (Pharm Lyse; BD Biosciences). Cells were counted, incubated with Fc block (1 h; BD Biosciences; 1:100 10^{-6} cells), incubated with fixable live/dead stain (30 min; Invitrogen), and then incubated with conjugated antibodies (1h). Alternatively, DAPI was used for dead cell exclusion instead of fixable live/dead stain. Antibodies and dilutions are listed in Supplementary Table 3. Mouse neutrophils were defined as CD45^{+}CD11b^{+}Gr1$^{+/hi}$ or CD45^{+}CD11b^{+}Ly6C^{lo}Ly6G^{+}. CD45^{+}CD11b^{+}Gr1^{lo} cells were determined to be CD45+CD11b+Ly6C^{hi} monocytes, and were therefore excluded from all neutrophil gating. OneComp eBeads (eBioscience) or ArC Amine Reactive Compensation Beads (Invitrogen) were used for compensation. A BD LSRFortessa was used for flow cytometry, and a BD FACSAria III was used for FACS. FlowJo was used for all flow cytometry and FACS data analysis, and for generating representative flow plots. For mouse cell gating strategy, in all cases, dead cells and debris were excluded from analyses using FSC × SSC, a live/dead stain and/or DAPI. CD45^{+} was used as a marker for total leukocytes; CD11b^{+} was used as a marker for myeloid cells. Neutrophils were further defined as CD45^{+}CD11b^{+}Gr1$^{+/hi}$ or CD45^{+}CD11b^{+}Ly6C^{lo}Ly6G^{+}. CD45^{+}CD11b^{+}Gr1^{lo} cells were determined to be CD45^{+}CD11b^{+}Ly6C^{hi} monocytes, and were therefore excluded from all neutrophil gating. Eosinophils were defined as CD45^{+}CD11b^{+} myeloid cells with high side scatter, and Siglec-f^{+}. In some cases, further gating on IL5ra^{+} or Ki67^{+} populations was performed for eosinophils, monocytes and neutrophils as defined here. T cells were gated as CD45^{+}CD3^{+} and then further gated according to positive CD4 or CD8 status for helper and cytotoxic T cells, respectively. For NK cell cytotoxicity assays, NK cells were defined as CD45^{+} with low side scatter, and NK1.1^{+}. Gating on CD107a^{+} populations was used to further define NK cells with cytotoxic function.

Flow cytometry of human blood samples.

Blood collection from human donors was approved by the Institutional Review Board of Rockefeller University, fully compliant with all relevant ethical regulations regarding research involving human participants, and obtained with informed consent. Fresh whole-blood samples were obtained from healthy female donors (including 5 lean donors, and 2 obese donors with BMI ≥ 35; donors were all postmenopausal) at Rockefeller University. Red blood cells were lysed directly (Pharm Lyse, BD Biosciences), cells were counted,

incubated with human Fc block (1 h; BD Biosciences; 1:100 10^{-6} cells), incubated with conjugated antibodies (1 h), and stained with DAPI (10 min). Antibodies and dilutions are listed in Supplementary Table 3. Cell surface markers were used to define different cell populations as follows: peripheral blood neutrophils ($CD45^+CD11b^+CD66b^+CD16^+CD14^{lo}$), eosinophils ($CD45^+CD11b^+CD66b^+CD16^-CD14^{lo}$), non-classical monocytes ($CD45^+CD11b^+CD66b^-CD16^+CD14^{lo}$), intermediate monocytes ($CD45^+CD11b^+CD66b^-CD16^+CD14^{hi}$) and classical monocytes ($CD45^+CD11b^+CD66b^-CD16^-CD14^+$). An antibody targeting IL5Rα was also included for all staining. Eosinophils were used as a positive gating control for IL5Rα positivity as this is a canonical marker/signalling pathway for this cell type[53].

Primary tumour growth and spontaneous metastasis.

To investigate the effects of obesity on breast cancer primary tumour growth, 1.5×10^6 breast cancer cells (86R2 or 99LN) were injected into the right thoracic mammary fat pad (MFP) of 20-week-old female DIO BL6 mice (that is, 15 weeks of feeding starting at 5 weeks old). Cells were injected in 1:1 serum-free DMEM/growth factor-reduced Matrigel (BD Biosciences). Tumour volume was measured by digital calliper and calculated as $V = (L \times W^2)/2$. Key time points throughout the trial were: 0 d, prior to tumour cell injection; 14 d, when primary tumours were first palpable; 28 d, before tumours had metastasized to lung; and 56 d, when lung micro-metastases were first evident. To assess spontaneous metastasis to lung, mice were euthanized at the 56 d time point, and lungs were perfused through the trachea with 10% formalin, paraffin-embedded, and stained with H&E. Tissue sections (10 mm^3) were scanned (that is, whole-lung cross-sections) and micro-metastases were counted manually using a Leica Aperio digital pathology slide scanner and analysis software. Primary tumour growth and spontaneous metastasis experiments were approved by RARC and IACUC and were performed in a manner compliant with all relevant ethical regulations regarding animal research.

Experimental metastasis assay.

To investigate the effects of obesity on experimental metastasis to lung, 2×10^6 99LN breast cancer cells labelled with GFP and luciferase (GFP-Luc) were injected into the tail vein of 20-week-old female DIO BL6 mice, or 11-week-old *ob/ob* mice. Cells were resuspended in calcium- and magnesium-free PBS, and filtered through a 40 μm mesh immediately prior to injection. Lung metastases were monitored for 48 h or 5 weeks using bioluminescent imaging (BLI; Xenogen IVIS-200 Optical In Vivo Imaging System). Luminescence was normalized to day 0 for each individual mouse, to account for any differences in injection efficiency between animals. Experimental metastasis experiments were approved by RARC and IACUC and were performed in a manner compliant with all relevant ethical regulations regarding animal research.

Neutralization of Gr1 or GM-CSF *in vivo*.

To target neutrophils in the DIO model, 5-week-old female WT BL6 mice were enrolled on HF or LF diet for 15 weeks, followed by antibody-mediated neutralization of Gr1 (6 μg g^{-1} body weight anti-Gr1 dosed every 3 d intraperitoneally, clone RB6-8C5, rat IgG2b isotype control; Tonbo Biosciences[9]) 3 d and 1 d prior to tail vein injection of 99LN breast tumour

cells (2×10^6 cells). This dosing regimen was confirmed by flow cytometry to efficiently deplete neutrophils in blood, spleen and lung for at least 3 d after each dose (that is, prior to and during the 48 h metastasis assay), using a Ly6C antibody that does not compete with the target antigen. The experimental metastasis assay was performed as described. For neutralization of GM-CSF, the same dosing regimen was used (16 μg g^{-1} body weight anti-GM-CSF dosed every 3 d intraperitoneally, clone MP122E9, rat IgG2a isotype control; R&D Systems[66]). Antibody neutralization experiments were approved by RARC and IACUC and were performed in a manner compliant with all relevant ethical regulations regarding animal research.

Recombinant GM-CSF preclinical trial.

To test whether GM-CSF alone is capable of modulating lung neutrophils, 5-week-old female WT BL6 mice enrolled on normal chow were treated with recombinant mouse GM-CSF (R&D Systems, 50 μg kg^{-1}, i.p. every day for 5 d, versus PBS control). After 5 d, mice were either euthanized and lung tissues harvested for flow cytometry analysis, or subjected to tail vein injection of 99LN breast tumour cells (2×10^6) for the 48 h experimental metastasis assay. During the experimental metastasis assay, mice were dosed via daily administration of GM-CSF. Recombinant protein treatment experiments were approved by RARC and IACUC and were performed in a manner compliant with all relevant ethical regulations regarding animal research.

Serum collection from mice and humans.

To collect serum from DIO mice, blood was collected by submandibular bleeding into Eppendorf tubes and allowed to clot at room temperature for ~20 min. Samples were centrifuged at 2,000*g*, 4 °C, 10 min. Supernatant was transferred to a polypropylene tube either individually or pooled. For pooled serum, three individual mouse samples were combined and stored at −80 °C for downstream applications. For human serum, samples were obtained as previously described from healthy female consenting donors[69], and banked as individual or pooled. Serum samples were pooled from 9 lean (BMI = 18–25) or 10 obese (BMI > 35) postmenopausal women (median age = 56 years old; age range 45–66) and stored at −80 °C for downstream application. For collection of matched human weight loss serum samples, the clinical trial was conducted at Rockefeller University under ClinicalTrials.gov identifier . Sample collection was approved by the Institutional Review Board of Rockefeller University (New York, USA). Mean BMI before weight loss = 38.8 ± 3.4 s.d.; mean BMI after weight loss = 35.1 ± 3.0 s.d.; mean age = 60.6 years ± 3.6 s.d.

In vitro myelopoiesis assay.

To harvest bone marrow cells, femurs and tibiae from WT BL6 mice were flushed under sterile conditions. Cells were filtered through a 40 μm mesh and cultured in Teflon bags (PermaLife PL-30) for 6 d in DMEM supplemented with 5% FBS, or 5% serum derived from either LF/HF mice or lean/obese humans. Recombinant proteins (CCL25, CD40L, GM-CSF, IGFBP2, IL5, IL6, MMP3, MMP9, 100 ng ml^{-1} for all; R&D Systems) or neutralization antibodies (IgG versus anti-GM-CSF, 0.1 μg ml^{-1}) were added as indicated. Treatment media were changed every other day. After 6 d, flow cytometry was performed using antibodies against murine CD45, CD11b and Gr1 (see Supplementary Table 3).

Cytokine arrays.

Cytokine arrays were purchased from RayBiotech (Mouse Cytokine Array G2000 and Human Cytokine Array G4000). The mouse G2000 series detects 144 cytokines and the human G4000 series detects 274 cytokines, of which 103 overlapping cytokines were included for downstream analysis. For both species, replicate samples contained pooled serum (9 pooled lean individuals and 10 pooled obese individuals per replicate for human, and 3 pooled animals per replicate for mouse). For each species, 2 independently pooled replicate samples were used, each run in duplicate, and P values were calculated on the basis of these 4 signal outputs. $P < 0.05$ was considered as statistically significant, and fold cutoff was not used. Both array series were performed according to the manufacturer's instructions. For a complete list of array results, see Supplementary Table 2.

ELISA analysis of serum GM-CSF and IL5 in mice and humans.

Human and Mouse IL5 and GM-CSF Quantikine ELISA kits were obtained from R&D Systems (catalogue no.: Human IL5 no. D5000B; human GM-CSF no. DGM00; mouse IL5 no. M5000; mouse GM-CSF no. MGM00), and ELISAs were performed according to the manufacturer's protocol. An Eppendorf Plate Reader AF2200 was used for colorimetric quantification and analysis at 460 nm and 570 nm wavelengths.

Invasion and migration assays.

For invasion assays, growth factor-reduced Matrigel (BD Biosciences) and serum-free DMEM were mixed at a 1:1 ratio, applied to Transwell inserts, and allowed to polymerize for >1 h. Fifty thousand cells were seeded in serum-free DMEM in the upper chamber, and DMEM + 5% FBS was added to the lower chamber. Cell invasion through the Transwell was counted manually after 24 h, by staining with DAPI and mounting. For cell migration assays, the same protocol was followed, except that Transwell chambers were not coated with Matrigel.

Adoptive transfer of neutrophils *in vivo*.

Adoptive cell transfer trial design was based on previously published methods[70]. Schematic representation of the trial design can be found in Fig. 7a. Briefly, bone marrow was collected from $n = 10$ WT or *ob/ob* mice, and neutrophils were enriched using a mouse Neutrophil Isolation Kit (Miltenyi Biotec). WT neutrophils were labelled with green fluorescent CellTrace dye and *ob/ob* neutrophils were labelled with far red fluorescent CellTrace dye (Invitrogen). WT and *ob/ob* neutrophils were mixed at an equal ratio (confirmed by flow cytometry), and then 3×10^6 cells were injected via tail vein into WT, *ob/ob* or *ob/ob* mice + neutralizing antibody against IL5 (1 mg kg^{-1} body weight, dosed 3 d and 1 d prior to adoptive transfer intravenously, clone TRFK5, rat IgG1 isotype control; R&D Systems)[67]. Blood and lungs were collected for flow cytometry after 4 h and 8 h, to evaluate homing and turnover, respectively. Adoptive transfer experiments were approved by RARC and IACUC and were performed in a manner compliant with all relevant ethical regulations regarding animal research.

T-cell CFSE assay.

T-cell proliferation was assessed by CFSE (Invitrogen) according to the manufacturer's protocol and published methods[9,43]. Briefly, CD8+ cytotoxic T cells were isolated from WT mice, stimulated with mouse T-Activator CD3/CD28 Dynabeads (ThermoFisher Scientific) and recombinant IL2 (30 U ml^{-1}; R&D Systems), and seeded (8×10^4 cells per well of 96-well plate) either alone or in co-culture with lung neutrophils isolated from LF- or HF-fed DIO mice at a ratio of 1:2. Culture media contained RPMI 1640 + 10% heat-inactivated FBS (Gibco), 1% P/S, 10 ml non-essential amino acid supplement, 200 mM L-glutamine, 100 mM sodium pyruvate, 1 M HEPES, and 5 μl β-mercaptoethanol. Co-culture was performed for 4 d prior to flow cytometry analysis of CFSE dye dilution, representing T-cell division.

NK cell cytotoxicity assay.

To assess the effect of neutrophils on NK cell cytotoxicity *in vitro*, $NK1.1^+$ cells were isolated by FACS from peripheral blood of WT BL6 mice, and were co-cultured for 3 d in a low-attachment dish at a 1:1 ratio with LF or HF peripheral neutrophils. Flow cytometry was used to quantify the expression of the degranulation marker CD107a on NK cells in response to co-culture. Culture media contained RPMI 1640 + 10% heat-inactivated FBS (Gibco), 1% P/S, 10 ml non-essential amino acid supplement, 200 mM L-glutamine, 100 mM sodium pyruvate, 1 M HEPES and 5 μl β-mercaptoethanol. To assess the effect of obesity on NK cell cytotoxicity *in vivo*, flow cytometry was used to quantify peripheral blood $NK1.1^+CD107a^+$ cells in tumour-bearing LF or HF mice.

RNA isolation and qRT-PCR.

RNA was isolated with Trizol, DNase treated, and 1 μg of RNA was used for cDNA synthesis using a High Capacity cDNA Reverse Transcription kit (Applied Biosystems). Mouse Taqman probes (Applied Biosystems) were used for quantifying expression of *Erbb2* (Mm00658541_m1), *Esr1* (Mm00433149_m1), *Pgr* (Mm00435628_m1), *Cdh1* (Mm01247357_m1), *Snai1* (Mm00441533_g1), *Snai2* (Mm00441531_m1), *Twist1* (Mm00442036_m1), *Vim* (Mm01333430_m1), *Zeb1* (Mm00495564_m1), *Zeb2* (Mm00497193_m1), *Csf2* (Mm01290062_m1), *Cxcl2* (Mm00436450_m1), *Cxcl12* (Mm00445553_m1), *Cxcr4* (Mm01996749_s1), *Cxcr2* (Mm99999117_s1), *Tlr4* (Mm00445273_m1), *Arg1* (Mm00475988_m1), *Ccl5* (Mm01302427_m1), *Ccl2* (Mm00441242_m1), *Tgfb1* (Mm01178820_m1), *Il10* (Mm01288386_m1), *Nox2* (Cybb) (Mm01287743_m1), *Nos2* (iNOS) (Mm00440502_m1), *Ptger2* (EP2) (Mm00436051_m1), *Ptgs2* (Cox-2) (Mm00478374_m1), *Pdl1* (Mm00452054_m1), *Il1b* (Mm00434228_m1), *Nlrp3* (Mm00840904_m1), *Alox5* (Mm01182747_m1), *S100a8* (Mm01220132_g1), *S100a9* (Mm00656925_m1), *Ccl25* (Mm00436443_m1), *Cd40lg* (Mm00441911_m1), *Igfbp2* (Mm00492632_m1), *Il5* (Mm00439646_m1), *I16* (Mm00446190_m1), *Mmp3* (Mm00440295_m1), *Mmp9* (Mm00442991_m1), *Csf2rb* (Mm00655745_m1), *Csf2ra* (Mm00438331_g1), *Il5ra* (Mm00434284_m1), *Hprt* (Mm03024075_m1), *Gapdh* (Mm99999915_g1).

Statistics and reproducibility.

GraphPad Prism Pro5 was used for all data analysis. Data are presented as mean ± standard error (s.e.m.) or box and whisker plots (boxplots) unless indicated otherwise, and $P < 0.05$ was considered as statistically significant. For all boxplots, the centre line is the median value, and the box extends from the 25th to 75th percentile. Whiskers and error bars are defined in the legends. For all representative images, results were reproduced at least 3 times in independent experiments. For all quantitative data, the statistical test used is indicated in the legends. Briefly, Gaussian distribution was first determined using the D'Agostino–Pearson omnibus normality test. Data that were determined to be parametric were analysed by a two-tailed unpaired Student's *t*-test (2 groups), or an ordinary one-way ANOVA (> 2 groups) with Dunnett's multiple comparisons test (that is, all groups compared with a control) or Bonferroni's multiple comparisons test (that is, select pairwise comparisons). Data that were determined to be non-parametric were analysed by a Mann–Whitney test (2 groups), or Kruskal–Wallis test (>2 groups) with Dunn's multiple comparisons. For animal studies, data were generated from at least 2 independent cohorts. For human weight loss studies, data were analysed by a two-tailed, paired Student's *t*-test to account for matched pre- and post-weight loss samples for each individual. All data included in the study are reproducible: all flow cytometry experiments were repeated 3 or more times with similar results; all animal trials were repeated with at least $n = 4$ in at least 2 independent cohorts with similar results; all *in vitro* assays were repeated in at least 3 independent experiments with similar results.

Data availability.

All data are available from the authors upon reasonable request. Statistical source data for Figs 2a, 4b,c,e, 5e–g and 8a–c,e,f and Supplementary Fig. 1c,d and Supplementary Fig. 2e are provided as Supplementary Table 4.

Supplementary Material

Refer to Web version on PubMed Central for supplementary material.

ACKNOWLEDGEMENTS

We thank members of the Joyce and Dannenberg laboratories and V. Mittal for insightful comments and discussion. We acknowledge J. O. Alemán for assistance in providing human sera from weight loss trials. We thank H.-W. Wang for originally isolating the PyMT-BL6 cell lines used herein, and F. Klemm and J. Kowal for critically reading the manuscript. This research was supported by the Breast Cancer Research Foundation (J.A.J., A.J.D.), the Ludwig Institute for Cancer Research (J.A.J.), NIH/NCI U54 CA210184-01 (A.J.D.), the Botwinick-Wolfensohn Foundation (in memory of Mr and Mrs Benjamin Botwinick) (A.J.D.), the Sackler Center for Biomedicine and Nutrition Research at The Rockefeller University (P.R.H.), a National Cancer Institute Cancer Center Support Grant awarded to MSKCC (P30 CA008748), and fellowships from the Canadian Institutes of Health Research (D.F.Q., L.A.W.), National Cancer Institute F31CA171384 (O.C.O.), and the American Brain Tumor Association in honour of Joel A. Gingras (L.A.).

References

1. Quail DF & Joyce JA Microenvironmental regulation of tumor progression and metastasis. Nat. Med 19, 1423–1437 (2013) [PubMed: 24202395]
2. Hanahan D & Weinberg RA Hallmarks of cancer: the next generation. Cell 144, 646–674 (2011) [PubMed: 21376230]

3. McAllister SS & Weinberg RA The tumour-induced systemic environment as a critical regulator of cancer progression and metastasis. Nat. Cell Biol 16, 717–727 (2014) [PubMed: 25082194]
4. Peinado H et al. Pre-metastatic niches: organ-specific homes for metastases. Nat. Rev. Cancer 17, 302–317 (2017) [PubMed: 28303905]
5. Grivennikov SI, Greten FR & Karin M Immunity, inflammation, and cancer. Cell 140, 883–899 (2010) [PubMed: 20303878]
6. Calle EE & Kaaks R Overweight, obesity and cancer: epidemiological evidence and proposed mechanisms. Nat. Rev. Cancer 4, 579–591 (2004) [PubMed: 15286738]
7. Ligibel JA et al. American Society of Clinical Oncology position statement on obesity and cancer. J. Clin. Oncol 32, 3568–3574 (2014) [PubMed: 25273035]
8. Fantuzzi G Adipose tissue, adipokines, and inflammation. J. Allergy Clin. Immunol 115, 911–919 (2005) [PubMed: 15867843]
9. Xia S et al. Gr-1^+ $CD11b^+$ myeloid-derived suppressor cells suppress inflammation and promote insulin sensitivity in obesity. J. Biol. Chem 286, 23591–23599 (2011) [PubMed: 21592961]
10. Kanneganti TD & Dixit VD Immunological complications of obesity. Nat. Immunol 13, 707–712 (2012) [PubMed: 22814340]
11. Iyengar NM, Hudis CA & Dannenberg AJ Obesity and inflammation: new insights into breast cancer development and progression. Am. Soc. Clin. Oncol. Educ. Book 33, 46–51 (2013)
12. Iyengar NM et al. Systemic correlates of white adipose tissue inflammation in early-stage breast cancer. Clin. Cancer Res 22, 2283–2289 (2015) [PubMed: 26712688]
13. Coussens LM & Werb Z Inflammation and cancer. Nature 420, 860–867 (2002) [PubMed: 12490959]
14. Ewertz M et al. Effect of obesity on prognosis after early-stage breast cancer. J. Clin. Oncol 29, 25–31 (2011) [PubMed: 21115856]
15. Osman MA & Hennessy BT Obesity correlation with metastases development and response to first-line metastatic chemotherapy in breast cancer. Clin. Med. Insights Oncol 9, 105–112 (2015) [PubMed: 26628862]
16. Khandekar MJ, Cohen P & Spiegelman BM Molecular mechanisms of cancer development in obesity. Nat. Rev. Cancer 11, 886–895 (2011) [PubMed: 22113164]
17. Weigelt B, Peterse JL & van 't Veer LJ Breast cancer metastasis: markers and models. Nat. Rev. Cancer 5, 591–602 (2005) [PubMed: 16056258]
18. Mancuso P Obesity and lung inflammation. J. Appl. Physiol 108, 722–728 (2010) [PubMed: 19875709]
19. Julia V, Macia L & Dombrowicz D The impact of diet on asthma and allergic diseases. Nat. Rev. Immunol 15, 308–322 (2015) [PubMed: 25907459]
20. Lackey DE & Olefsky JM Regulation of metabolism by the innate immune system. Nat. Rev. Endocrinol 12, 15–28 (2016) [PubMed: 26553134]
21. Catena R et al. Bone marrow-derived $Gr1^+$ cells can generate a metastasis-resistant microenvironment via induced secretion of thrombospondin-1. Cancer Discov 3, 578–589 (2013) [PubMed: 23633432]
22. Liu Y et al. Tumor exosomal RNAs promote lung pre-metastatic niche formation by activating alveolar epithelial TLR3 to recruit neutrophils. Cancer Cell 30, 243–256 (2016) [PubMed: 27505671]
23. Gao D et al. Myeloid progenitor cells in the premetastatic lung promote metastases by inducing mesenchymal to epithelial transition. Cancer Res. 72, 1384–1394 (2012) [PubMed: 22282653]
24. Wculek SK & Malanchi I Neutrophils support lung colonization of metastasis-initiating breast cancer cells. Nature 528, 413–417 (2015) [PubMed: 26649828]
25. Casbon AJ et al. Invasive breast cancer reprograms early myeloid differentiation in the bone marrow to generate immunosuppressive neutrophils. Proc. Natl Acad. Sci. USA 112, E566–E575 (2015) [PubMed: 25624500]
26. Sharma SK et al. Pulmonary alveolar macrophages contribute to the premetastatic niche by suppressing antitumor T cell responses in the lungs. J. Immunol 194, 5529–5538 (2015) [PubMed: 25911761]

27. Coffelt SB et al. IL-17-producing γδ T cells and neutrophils conspire to promote breast cancer metastasis. Nature 522, 345–348 (2015) [PubMed: 25822788]
28. Qian BZ et al. CCL2 recruits inflammatory monocytes to facilitate breast-tumour metastasis. Nature 475, 222–225 (2011) [PubMed: 21654748]
29. Kowanetz M et al. Granulocyte-colony stimulating factor promotes lung metastasis through mobilization of Ly6G+Ly6C+ granulocytes. Proc. Natl Acad. Sci. USA 107, 21248–21255 (2010) [PubMed: 21081700]
30. Zhang Y et al. Positional cloning of the mouse obese gene and its human homologue. Nature 372, 425–432 (1994) [PubMed: 7984236]
31. Montgomery MK et al. Mouse strain-dependent variation in obesity and glucose homeostasis in response to high-fat feeding. Diabetologia 56, 1129–1139 (2013) [PubMed: 23423668]
32. Gabrilovich DI, Ostrand-Rosenberg S & Bronte V Coordinated regulation of myeloid cells by tumours. Nat. Rev. Immunol 12, 253–268 (2012) [PubMed: 22437938]
33. Delano MJ et al. Neutrophil mobilization from the bone marrow during polymicrobial sepsis is dependent on CXCL12 signaling. J. Immunol 187, 911–918 (2011) [PubMed: 21690321]
34. Eash KJ, Greenbaum AM, Gopalan PK & Link DC CXCR2 and CXCR4 antagonistically regulate neutrophil trafficking from murine bone marrow. J. Clin. Invest 120, 2423–2431 (2010) [PubMed: 20516641]
35. Fan J & Malik AB Toll-like receptor-4 (TLR4) signaling augments chemokine-induced neutrophil migration by modulating cell surface expression of chemokine receptors. Nat. Med 9, 315–321 (2003) [PubMed: 12592402]
36. Fridlender ZG et al. Polarization of tumor-associated neutrophil phenotype by TGF-β: “N1” versus “N2” TAN. Cancer Cell 16, 183–194 (2009) [PubMed: 19732719]
37. Granot Z et al. Tumor entrained neutrophils inhibit seeding in the premetastatic lung. Cancer Cell 20, 300–314 (2011) [PubMed: 21907922]
38. Bronte V et al. IL-4-induced arginase 1 suppresses alloreactive T cells in tumorbearing mice. J. Immunol 170, 270–278 (2003) [PubMed: 12496409]
39. Kusmartsev S, Nefedova Y, Yoder D & Gabrilovich DI Antigen-specific inhibition of CD8+ T cell response by immature myeloid cells in cancer is mediated by reactive oxygen species. J. Immunol 172, 989–999 (2004) [PubMed: 14707072]
40. Sinha P, Clements VK, Fulton AM & Ostrand-Rosenberg S Prostaglandin E2 promotes tumor progression by inducing myeloid-derived suppressor cells. Cancer Res 67, 4507–4513 (2007) [PubMed: 17483367]
41. Nagareddy PR et al. Adipose tissue macrophages promote myelopoiesis and monocytosis in obesity. Cell Metab. 19, 821–835 (2014) [PubMed: 24807222]
42. Sinha P et al. Proinflammatory S100 proteins regulate the accumulation of myeloid-derived suppressor cells. J. Immunol 181, 4666–4675 (2008) [PubMed: 18802069]
43. Spiegel A et al. Neutrophils suppress intraluminal NK cell-mediated tumor cell clearance and enhance extravasation of disseminated carcinoma cells. Cancer Discov. 6, 630–649 (2016) [PubMed: 27072748]
44. Yan HH et al. Gr-1+CD11b+ myeloid cells tip the balance of immune protection to tumor promotion in the premetastatic lung. Cancer Res. 70, 6139–6149 (2010) [PubMed: 20631080]
45. Sevenich L et al. Analysis of tumour- and stroma-supplied proteolytic networks reveals a brain-metastasis-promoting role for cathepsin S. Nat. Cell Biol 16, 876–888 (2014) [PubMed: 25086747]
46. Herishanu Y, Rogowski O, Polliack A & Marilus R Leukocytosis in obese individuals: possible link in patients with unexplained persistent neutrophilia. Eur. J. Haematol 76, 516–520 (2006) [PubMed: 16696775]
47. Dranoff G et al. Involvement of granulocyte-macrophage colony-stimulating factor in pulmonary homeostasis. Science264, 713–716 (1994) [PubMed: 8171324]
48. Stanley E et al. Granulocyte/macrophage colony-stimulating factor-deficient mice show no major perturbation of hematopoiesis but develop a characteristic pulmonary pathology. Proc. Natl Acad. Sci. USA 91, 5592–5596 (1994) [PubMed: 8202532]

49. Uchida K et al. GM-CSF autoantibodies and neutrophil dysfunction in pulmonary alveolar proteinosis. N. Engl. J. Med 356, 567–579 (2007) [PubMed: 17287477]
50. Hoshi H et al. IL-5, IL-8 and GM-CSF immunostaining of sputum cells in bronchial asthma and chronic bronchitis. Clin. Exp. Allergy 25, 720–728 (1995) [PubMed: 7584683]
51. Lambrecht BN & Hammad H The immunology of asthma. Nat. Immunol. 16, 45–56 (2015) [PubMed: 25521684]
52. Asquith KL et al. The IL-3/IL-5/GM-CSF common receptor plays a pivotal role in the regulation of Th2 immunity and allergic airway inflammation. J. Immunol 180, 1199–1206 (2008) [PubMed: 18178860]
53. Rosenberg HF, Dyer KD & Foster PS Eosinophils: changing perspectives in health and disease. Nat. Rev. Immunol 13, 9–22 (2013) [PubMed: 23154224]
54. Linch SN et al. Interleukin 5 is protective during sepsis in an eosinophil-independent manner. Am. J. Respir. Crit. Care Med 186, 246–254 (2012) [PubMed: 22652030]
55. Hakonarson H, Maskeri N, Carter C, Chuang S & Grunstein MM Autocrine interaction between IL-5 and IL-1β mediates altered responsiveness of atopic asthmatic sensitized airway smooth muscle. J. Clin. Invest 104, 657–667 (1999) [PubMed: 10487780]
56. Tournoy KG, Kips JC & Pauwels RA The allergen-induced airway hyperresponsiveness in a human-mouse chimera model of asthma is T cell and IL-4 and IL-5 dependent. J. Immunol 166, 6982–6991 (2001) [PubMed: 11359860]
57. Wahl S et al. Epigenome-wide association study of body mass index, and the adverse outcomes of adiposity. Nature 541, 81–86 (2017) [PubMed: 28002404]
58. Alemán JO et al. Effects of rapid weight loss on systemic and adipose tissue inflammation and metabolism in obese postmenopausal women. J. Endocr. Soc 1, 625–637 (2017) [PubMed: 29264516]
59. Chen SB et al. Serum C-reactive protein and white blood cell count in morbidly obese surgical patients. Obes. Surg 19, 461–466 (2009) [PubMed: 18651197]
60. Cottam D et al. Tumor growth factor expression in obesity and changes in expression with weight loss: another cause of increased virulence and incidence of cancer in obesity. Surg. Obes. Relat. Dis 6, 538–541 (2010) [PubMed: 20688580]
61. Molofsky AB et al. Innate lymphoid type 2 cells sustain visceral adipose tissue eosinophils and alternatively activated macrophages. J. Exp. Med 210, 535–549 (2013). [PubMed: 23420878]
62. Brestoff JR et al. Group 2 innate lymphoid cells promote beiging of white adipose tissue and limit obesity. Nature 519, 242–246 (2015). [PubMed: 25533952]
63. Fainardi V, Pisi G & Chetta A Mepolizumab in the treatment of severe eosinophilic asthma. Immunotherapy 8, 27–34 (2016). [PubMed: 26653083]
64. Bhardwaj P et al. Caloric restriction reverses obesity-induced mammary gland inflammation in mice. Cancer Prev. Res 6, 282–289 (2013).
65. Pietrocola F et al. Caloric restriction mimetics enhance anticancer immunosurveillance. Cancer Cell 30, 147–160 (2016). [PubMed: 27411589]
66. Botelho FM et al. A mouse GM-CSF receptor antibody attenuates neutrophilia in mice exposed to cigarette smoke. Eur. Respir. J 38, 285–294 (2011). [PubMed: 21436349]
67. Zaynagetdinov R et al. Interleukin-5 facilitates lung metastasis by modulating the immune microenvironment. Cancer Res. 75, 1624–1634 (2015). [PubMed: 25691457]
68. Binder CJ et al. IL-5 links adaptive and natural immunity specific for epitopes of oxidized LDL and protects from atherosclerosis. J. Clin. Invest 114, 427–437 (2004). [PubMed: 15286809]
69. Esper RM et al. Leptin and adiponectin modulate the self-renewal of normal human breast epithelial stem cells. Cancer Prev. Res 8, 1174–1183 (2015).
70. Swamydas M & Lionakis MS Isolation, purification and labeling of mouse bone marrow neutrophils for functional studies and adoptive transfer experiments. J. Vis. Exp 77, e50586 (2013).

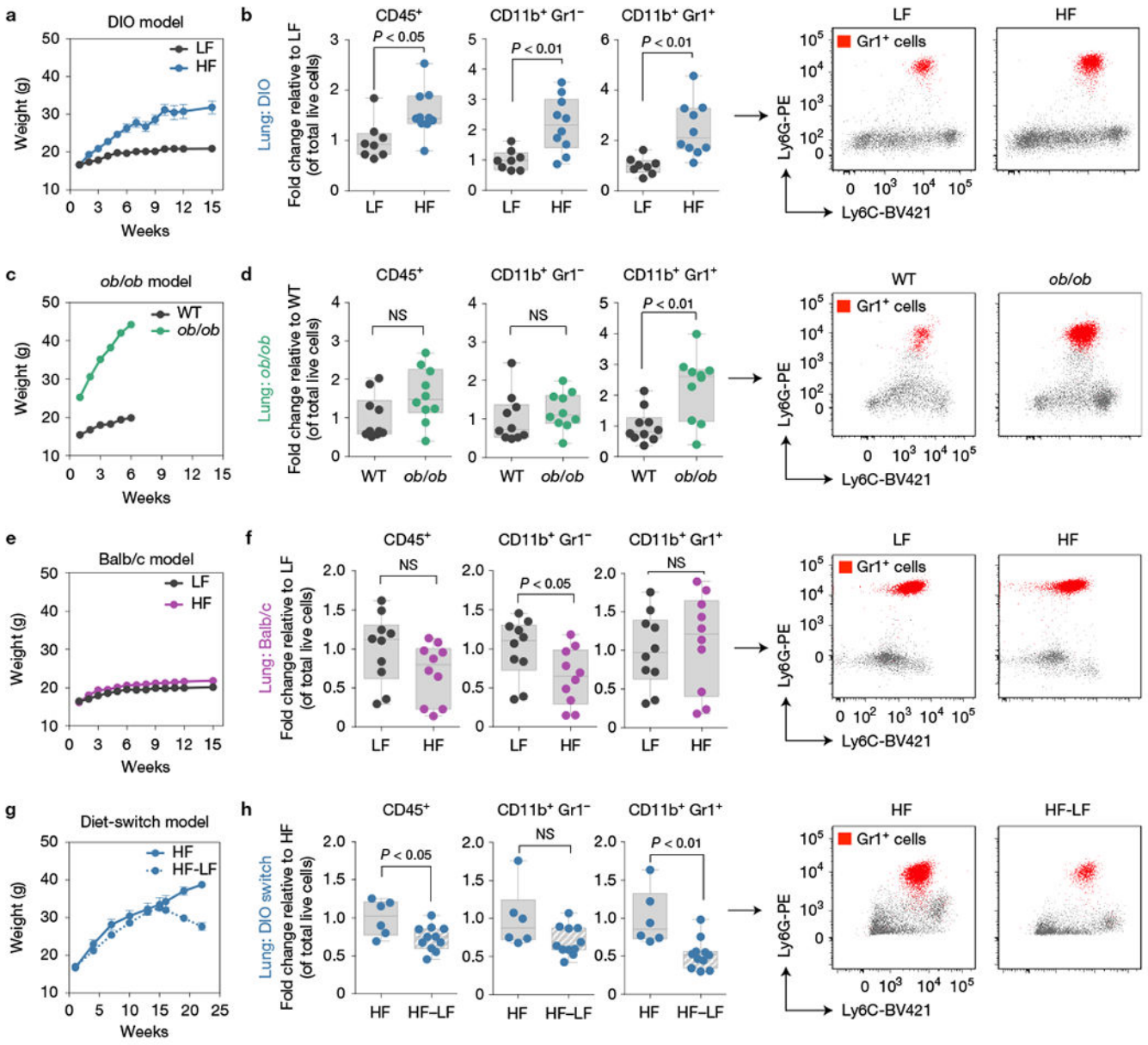

Figure 1.

Obesity is associated with lung neutrophilia driven by adiposity. (**a**) Weight curves for the diet-induced obesity (DIO) model. 5-week-old female BL6 mice were fed a low-fat (LF) or high-fat (HF) diet for 15 weeks. LF, $n = 8$ mice; HF, $n = 10$ mice; mean ± s.e.m. (**b**) Left, flow cytometry of lung myeloid cells in the DIO model at 15 weeks. LF, $n = 8$ mice; HF, $n = 10$ mice; minimum–maximum boxplots, all data points shown. Right, $CD11b^{+}Gr1^{+}$ populations are shown as a red overlay on total $CD11b^{+}$ cells, graphed on Ly6C (*x* axis) by Ly6G (*y* axis) dot plots. (**c**) Weight curves for the leptin-deficient genetic model of obesity (*ob/ob*). Female *ob/ob* or wild-type (WT) mice were fed a normal diet until the pre-defined weight endpoint of >40 g. $n = 10$ mice per group; mean ± s.e.m. (**d**) Left, flow cytometry of lung myeloid cells in the *ob/ob* model at 6 weeks. Representative plots (right) are displayed as in **b**. $n = 10$ mice per group; minimum–maximum boxplots, all data points shown. (**e**)

Weight curves for the obesity-resistant Balb/c model. 5-week-old female Balb/c mice were fed a LF or HF diet for 15 weeks. $n = 10$ mice per group; mean ± s.e.m. (**f**) Left, flow cytometry of lung myeloid cells in the Balb/c model at 15 weeks. Representative plots (right) are displayed as in **b**. $n = 10$ mice per group, minimum–maximum boxplots, all data points shown. (**g**) Weight curves for the diet-switch model. 5-week-old female BL6 mice were fed a HF diet over 15 weeks, and then switched to LF diet for an additional 7 weeks (HF–LF). HF, $n = 6$ mice; HF–LF, $n = 11$ mice; mean ± s.e.m. (**h**) Left, flow cytometry of lung myeloid cell subsets in the diet-switch model. Representative plots (right) are displayed as in **b**. HF, $n = 6$ mice; HF–LF, $n = 11$ mice, minimum–maximum boxplots, all data points shown. Significance was calculated via two-tailed unpaired Student's *t*-test throughout. NS, not significant. Box plots represent median and interquartile range while whiskers represent maximum and minimum values excluding outliers. Each symbol represents one mouse.

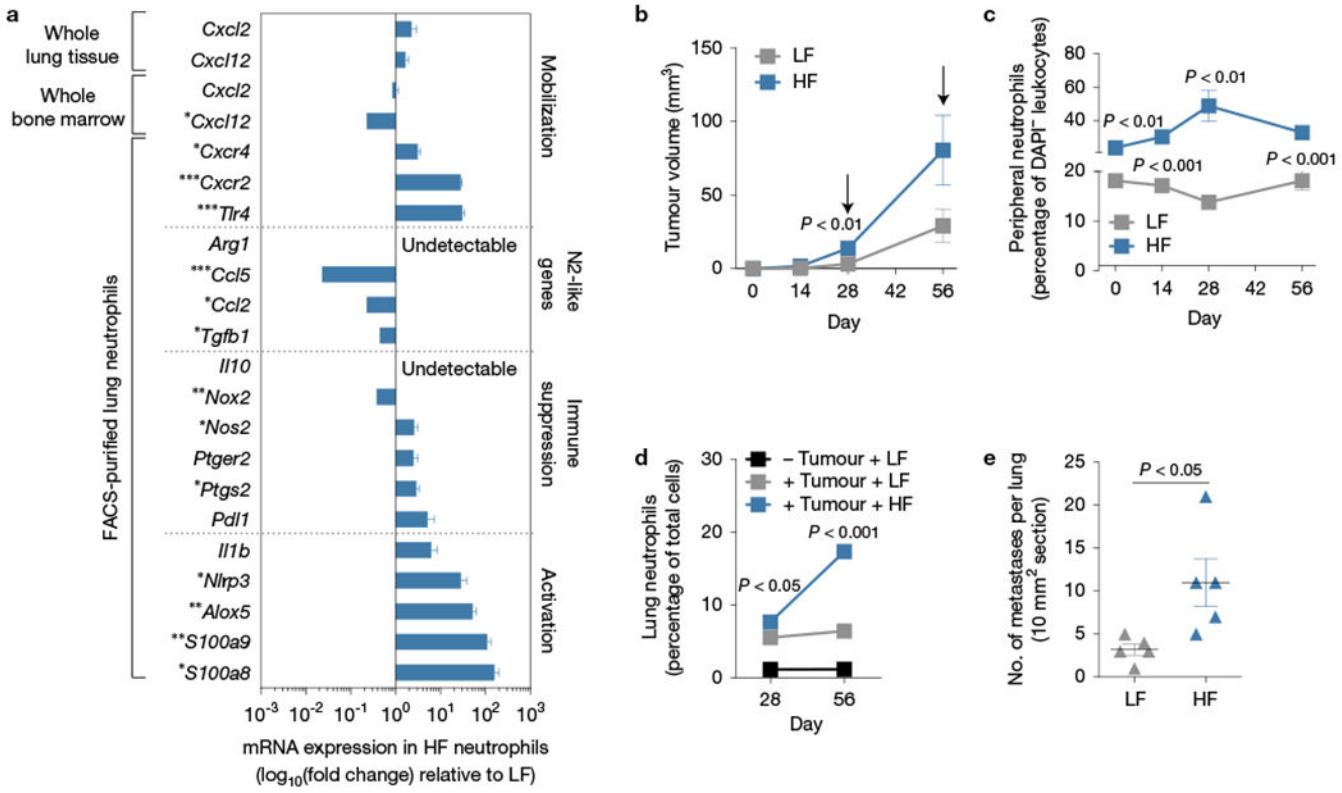

Figure 2.

Obesity-associated lung neutrophilia is accompanied by prometastatic gene expression changes and enhanced metastatic progression. (**a**) qRT-PCR on whole lung, bone marrow (BM) or FACS-purified lung neutrophils from HF non-tumour-bearing mice. Data are displayed as $\log_{10}$(fold change) relative to LF (centre normalized line). BM and whole lung, $n = 5$ mice; lung neutrophils, $n = 4$ mice. $^{*}P < 0.05$, $^{**}P < 0.01$, $^{***}P < 0.001$. (**b**) Primary tumour volume of 99LN cells injected via mammary fat pad (1.5×10^6 cells per mouse) in the DIO model. Key time points of primary tumour progression are presented: palpable (14 d, $n = 10$ mice), early phases of primary tumour growth (28 d, $n = 10$ mice; pre-metastatic niche), late phases of primary tumour growth (56 d, $n = 5$ mice; micro-metastatic disease). Arrows: $n = 5$ mice per group were euthanized at 28 d and at 56 d for analysis of lung neutrophilia, as in **d**. (**c**) Flow cytometry of blood neutrophils in tumour-bearing LF or HF mice over time. 0 d represents baseline circulating neutrophils prior to tumour cell injection. $n = 5$ mice per time point (matched from 0 d-56 d). (**d**) Flow cytometry of lung neutrophils in tumour-bearing LF or HF mice after 28 d or 56 d. Quantification of lung neutrophils in non-tumour-bearing LF mice is included as a control (black line). The reported P values indicate significant differences between tumour-bearing LF versus HF mice, $n = 5$ mice per group. (**e**) Quantification of spontaneous micro-metastases in lung at 56 d, $n = 5$ mice per group. Metastases were counted manually from scanned images of lung tissues, representing ~10 mm^2. All data are displayed as mean ± s.e.m.; significance calculated via two-tailed, unpaired Student's t-test throughout.

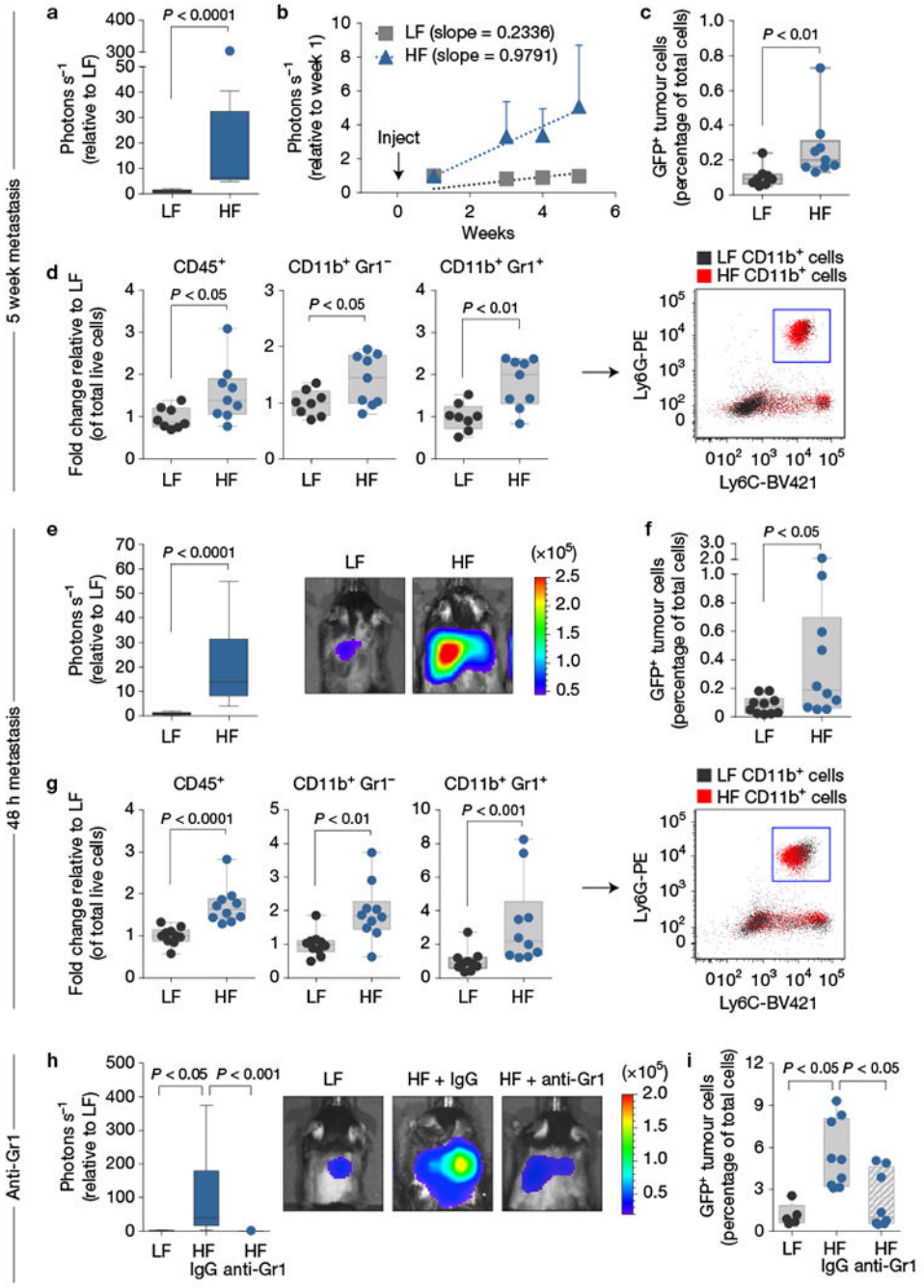

Figure 3.

Obesity enhances experimental breast cancer metastasis to lung in a neutrophil-dependent manner. (**a**) BLI of the 5 week metastasis assay with 99LN tumour cells injected via the tail vein into the DIO model. LF, $n = 8$ mice; HF, $n = 9$ mice; Tukey boxplot, Mann–Whitney test. (**b**) Weekly BLI over the 5 week metastasis experiment as shown in **a**. Mean ± s.e.m. (one-sided); dotted lines of best fit with corresponding slopes are displayed. (**c**) Flow cytometry of GFP$^+$ 99LN cells in DIO lung after the 5 week metastasis assay. LF, $n = 8$ mice; HF, $n = 9$ mice; minimum–maximum boxplots, all data points shown, Mann–Whitney

test. (**d**) Left, flow cytometry of lung myeloid cells in the 5 week metastasis assay. Right, representative dot plot shows total $CD11b^+$ cells from LF (grey) and HF (red) lungs, and double-positive $Ly6C^+$ $Ly6G^+$ cells (blue gate). LF, $n = 8$ mice; HF, $n = 9$ mice; minimum–maximum boxplots, all data points shown, two-tailed unpaired Student's *t*-test. (**e**) Left, BLI of the 48 h metastasis assay with 99LN cells injected via the tail vein into the DIO model. Right, representative images are shown. $n = 10$ mice per group; Tukey boxplot, Mann–Whitney test. (**f**) Flow cytometry of GFP^+ 99LN cells in DIO lung after 48 h metastasis assay. $n = 10$ mice per group; minimum–maximum boxplots, all data points shown, Mann–Whitney test. (**g**) Left, flow cytometry of lung myeloid cells in the 48 h metastasis assay. Right, representative plots are displayed as in **d**. $n = 10$ mice per group; minimum–maximum boxplots, all data points shown, Mann–Whitney test. (**h**) Left, BLI of the 48 h metastasis assay with 99LN cells injected via the tail vein into the DIO model, +/− a neutralization antibody against Gr1. Right, representative images are shown. LF, $n = 5$ mice; HF + IgG, $n = 9$ mice; HF + anti-Gr1, $n = 8$ mice; Tukey boxplot, Kruskal–Wallis and Dunn's multiple comparisons test. (**i**) Flow cytometry of GFP^+ 99LN cells in lung, corroborating results in **h**. LF, $n = 5$ mice; HF + IgG, $n = 9$ mice; HF + anti-Gr1, $n = 8$ mice; minimum–maximum boxplots, all data points shown, Kruskal–Wallis and Dunn's multiple comparisons test. Box plots represent median and interquartile range while whiskers represent maximum and minimum values excluding outliers. Each symbol represents one mouse.

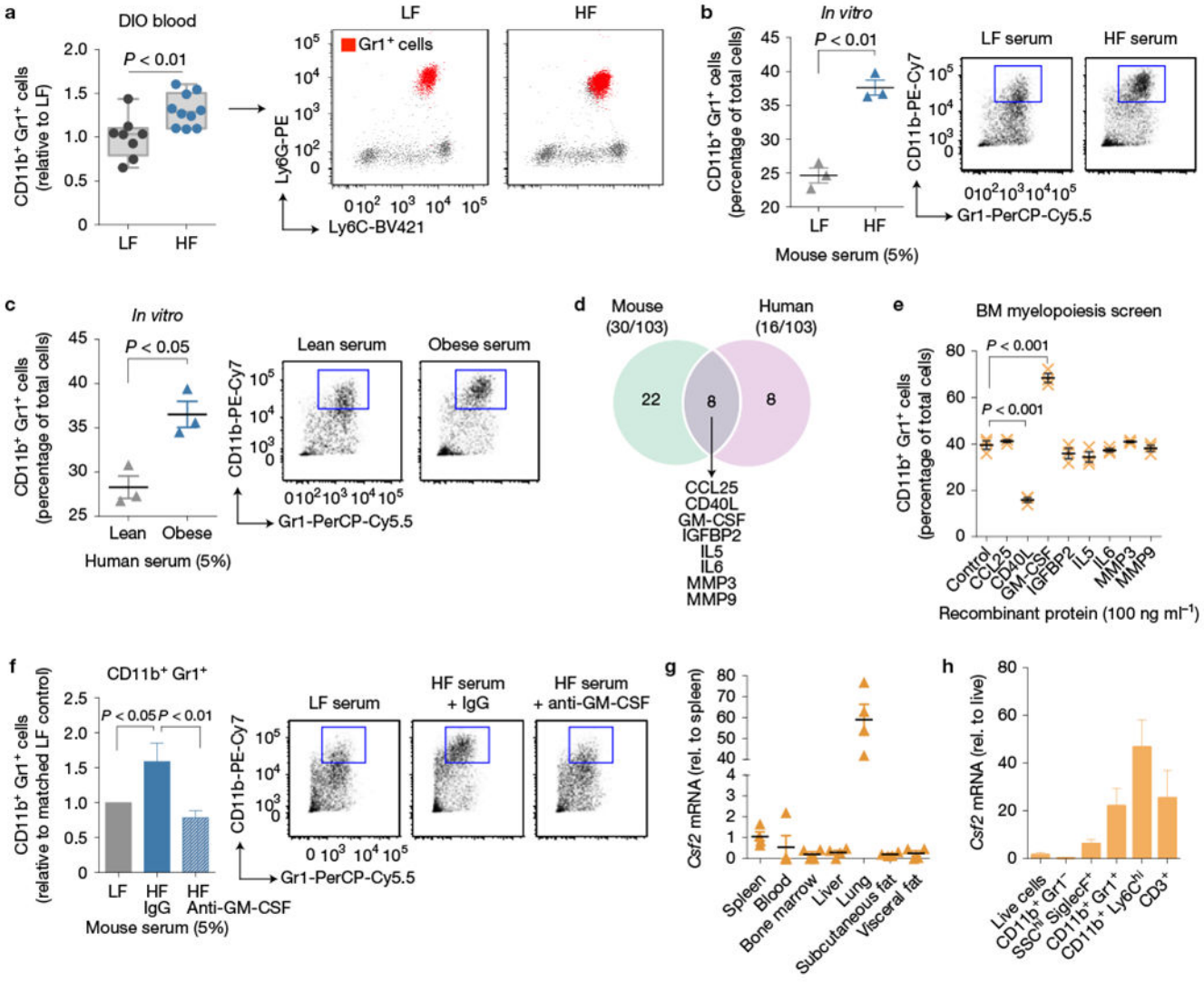

Figure 4.

Serum GM-CSF is elevated in obesity in association with CD11b$^+$Gr1$^+$ cells. (**a**) Left, flow cytometry of circulating CD11b$^+$Gr1$^+$ cells in the DIO model. Right, CD11b$^+$Gr1$^+$ populations are shown as a red overlay upon total CD11b$^+$ cells, graphed on Ly6C (*x* axis) by Ly6G (*y* axis) dot plots. LF, $n = 8$ mice; HF, $n = 10$ mice; minimum–maximum boxplots, all data points shown, two-tailed unpaired Student's *t*-test. (**b**) Left, *in vitro* myelopoiesis assay, demonstrating increased differentiation of mouse BM cells towards a CD11b$^+$Gr1$^+$ phenotype after treatment with HF serum compared with LF serum from the DIO model. $n =$ 3 independent BM isolations; mean ± s.e.m., two-tailed unpaired Student's *t*-test. Right, representative flow plots are shown. (**c**) Left, *in vitro* myelopoiesis assay, demonstrating increased differentiation of mouse BM cells towards a CD11b$^+$Gr1$^+$ phenotype after treatment with obese serum compared with lean serum from human donors. $n = 3$ independent BM isolations; mean ± s.e.m., two-tailed unpaired Student's *t*-test. Right, representative flow plots are shown. (**d**) Venn diagram of results from cross-species cytokine array (Supplementary Table 2). Out of 103 factors, 30 were elevated in HF versus LF mouse

serum, and 16 out of 103 factors were elevated in obese versus lean human serum. Eight overlapping factors were identified, including CCL25, CD40L, GM-CSF, IGFBP2, IL5, IL6, MMP3 and MMP9. (**e**) *In vitro* myelopoiesis assay, testing the capacity of the 8 factors identified in **d** to regulate BM differentiation towards a $CD11b^{+}Gr1^{+}$ phenotype. $n = 3$ independent mouse BM isolations; mean ± s.e.m., one-way ANOVA and Dunnett's multiple comparisons test. (**f**) *In vitro* myelopoiesis assay, demonstrating that GM-CSF neutralization reverses the effects of HF serum on $CD11b^{+}Gr1^{+}$ differentiation. $n = 6$ independent mouse BM isolations; mean ± s.e.m., one-way ANOVA and Dunnett's multiple comparisons test. (**g**) qRT-PCR of *Csf2* (GM-CSF) across different tissues in HF-fed animals. $n = 4$ mice per tissue; mean ± s.e.m. (**h**) qRT-PCR of *Csf2* in different FACS-purified cell types from HF lung tissues. $n = 5$ mice per cell type; mean ± s.e.m. Box plots represent median and interquartile range while whiskers represent maximum and minimum values excluding outliers. Each symbol represents one mouse.

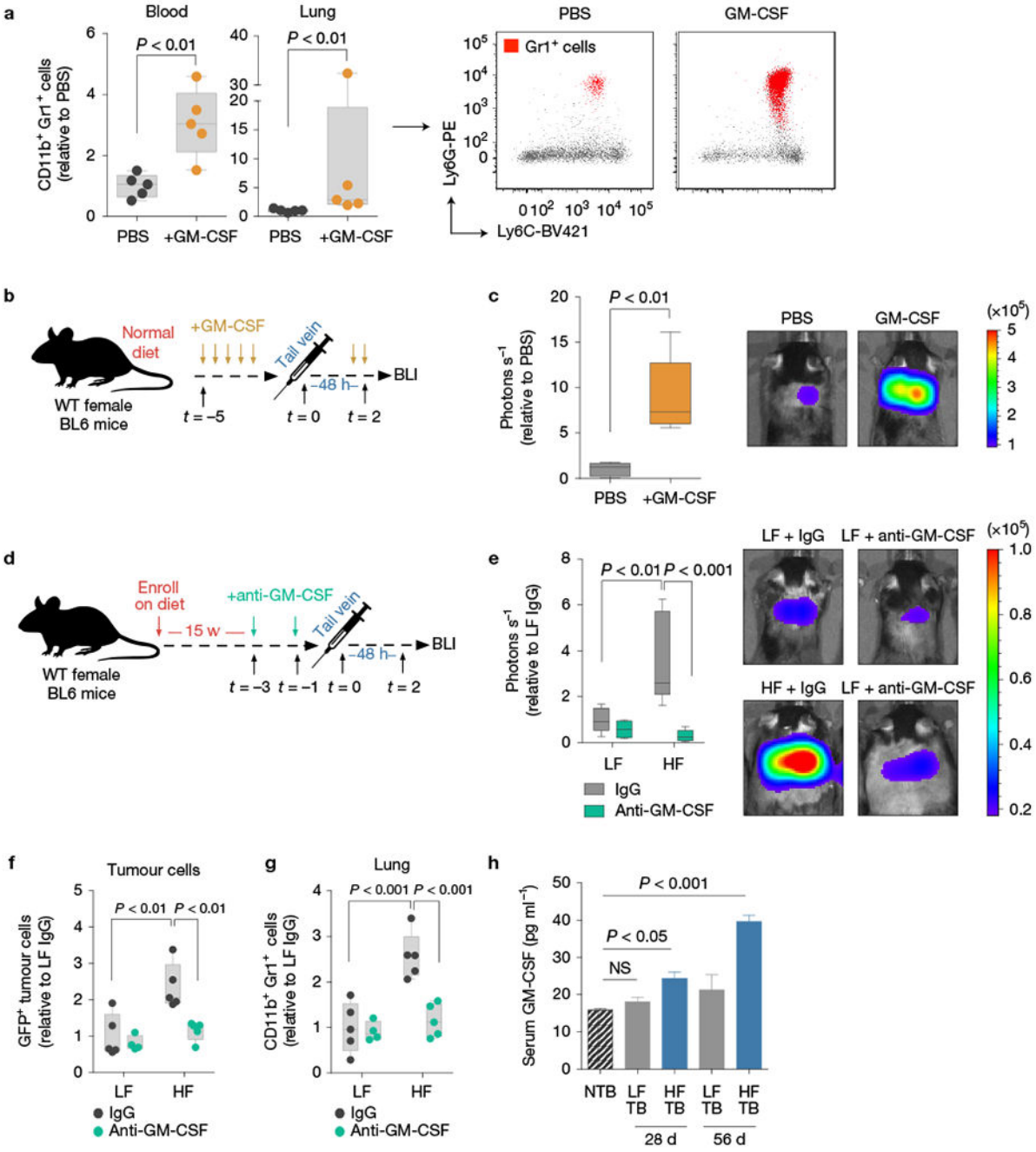

Figure 5.

GM-CSF underlies obesity-associated lung neutrophilia and breast cancer metastasis. (**a**) Left, flow cytometry of $CD11b^{+}Gr1^{+}$ cells in blood and lung from WT BL6 animals treated for 5 d with rGM-CSF versus PBS. $n = 5$ mice per group; minimum–maximum boxplot, all data points shown, Mann–Whitney test. Right, lung $CD11b^{+}Gr1^{+}$ populations are shown as a red overlay upon total $CD11b^{+}$ cells, graphed on Ly6C (x axis) by Ly6G (y axis) dot plots. (**b**) Trial schematic for **c**: daily rGM-CSF treatment (from day −5) followed by 99LN experimental metastasis assay (48 h; continued GM-CSF treatment). (**c**) Left, BLI

quantification of the trial depicted in **b**. Right, representative images are shown. *n* = 5 mice per group; Tukey boxplot, Mann–Whitney test. (**d**) Trial schematic for **e**–**g**: antibody-based GM-CSF neutralization (day −3 and −1) followed by 99LN experimental metastasis assay (48 h) in the DIO model. (**e**) Left, BLI quantification of the trial depicted in **d**. Right, representative images are shown. LF/HF + IgG, *n* = 5 mice; LF + anti-GM-CSF, *n* = 4 mice; HF + anti-GM-CSF, *n* = 5 mice; Tukey boxplot, one-way ANOVA and Bonferroni's multiple comparisons test. (**f**) Flow cytometry of GFP^+ 99LN cells in lung after the trial depicted in **d**. LF/HF + IgG, *n* = 5 mice; LF + anti-GM-CSF, *n* = 4 mice; HF + anti-GM-CSF, *n* = 5 mice; minimum–maximum, all data points shown, one-way ANOVA and Bonferroni's multiple comparisons test. (**g**) Flow cytometry of $CD11b^+Gr1^+$ cells in lung after the trial depicted in **d**. LF/HF + IgG, *n* = 5 mice; LF + anti-GM-CSF, *n* = 4 mice; HF + anti-GM-CSF, *n* = 5 mice; minimum–maximum, all data points shown, one-way ANOVA and Bonferroni's multiple comparisons test. (**h**) ELISA of serum GM-CSF in DIO mice with orthotopic breast tumours, corresponding to the trial from Fig. 2b. Serum was isolated from tumour-bearing (TB) LF or HF animals after 28 d (early; pre-metastatic disease) and 56 d (late; early micro-metastatic disease). Non-tumour-bearing (NTB) LF animals are included for comparison. *n* = 5 mice per group; mean ± s.e.m., one-way ANOVA and Dunnett's multiple comparisons test. NS, not significant. Box plots represent median and interquartile range while whiskers represent maximum and minimum values excluding outliers. Each symbol represents one mouse.

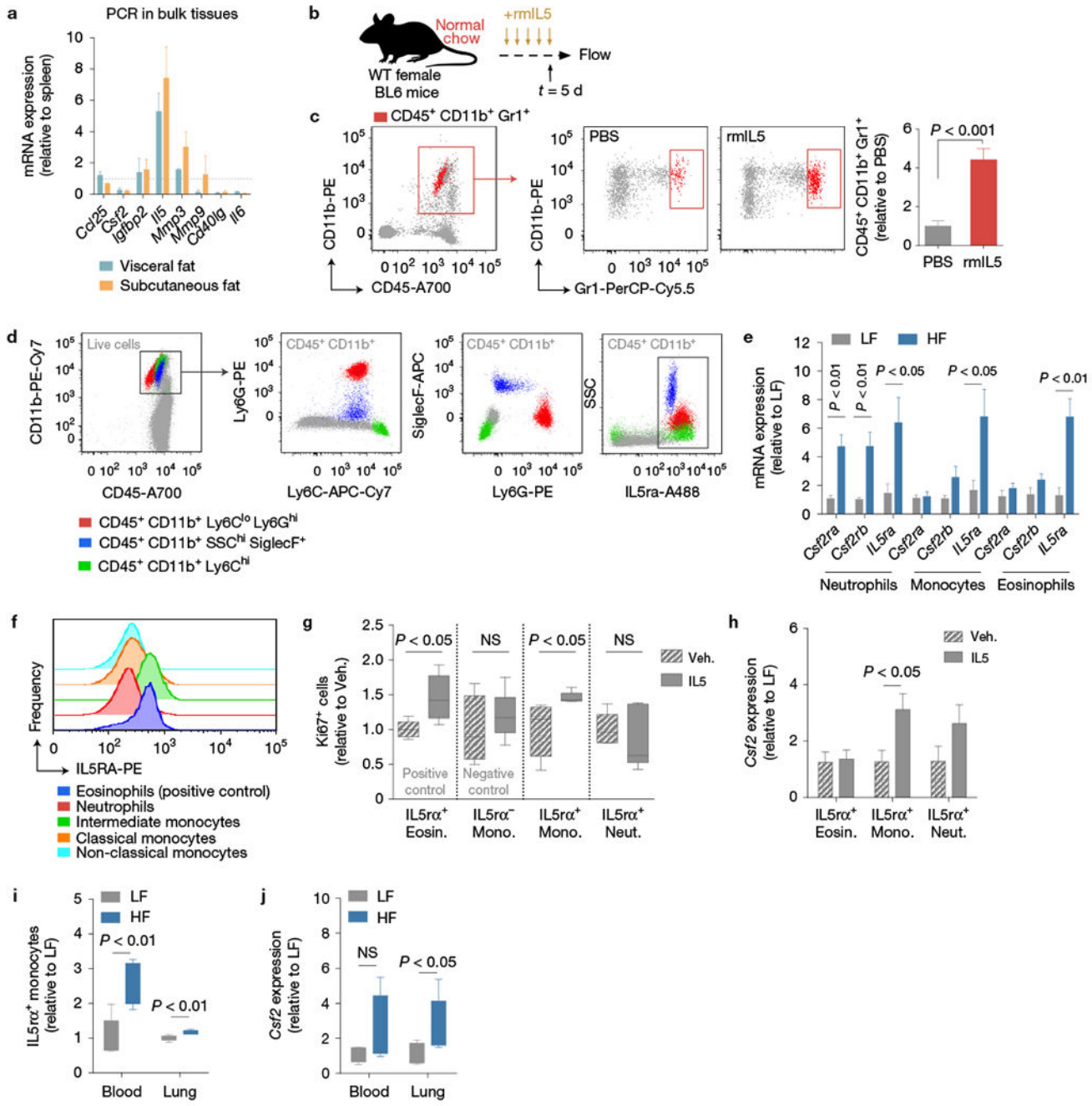

Figure 6.

IL5 signalling supports lung neutrophilia. (**a**) qRT–PCR of *Ccl25, Csf2, Igfbp2, Il5, Mmp3, Mmp9, Cd40lg* and *Il6* in visceral and subcutaneous fat from mice on HF diet. $n = 4$ mice per tissue; mean ± s.e.m. (**b**) Trial schematic for **c**: WT BL6 mice were treated daily with rIL5 or PBS (5 d), and immune cells in lung were quantified by flow cytometry. (**c**) Representative flow cytometry plots (left) and quantification (right) of lung neutrophils following the trial depicted in **b**. $n = 5$ mice per group; mean ± s.e.m., two-tailed unpaired Student's *t*-test. (**d**) Representative flow plots showing gating strategy and population

distribution for IL5Rα$^+$ cells. (**e**) qRT-PCR of *Csf2ra, Csf2rb* and *Il5ra* in FACS-purified lung neutrophils, monocytes and eosinophils from the DIO model. $n = 5$ mice per group; mean ± s.e.m., two-tailed unpaired Student's *t*-test. (**f**) Representative flow plots showing IL5Rα$^+$ populations in human blood. Eosinophils (blue) were used as a positive gating control, $n = 7$ healthy donors. (**g**) Quantification of cell proliferation *in vitro* in response to rIL5 treatment via flow cytometry for Ki67$^+$ cells. Cells isolated from $n = 5$ mice per group; Tukey boxplot, two-tailed unpaired Student's *t*-test. (**h**) qRT–PCR of *Csf2* expression in FACS-purified IL5Rα$^+$ cells after treatment with rIL5 *in vitro* (100 ng ml^{-1}, 4 h). Cells isolated from $n = 5$ mice per group; mean ± s.e.m., two-tailed unpaired Student's *t*-test. (**i**) Flow cytometry analysis of IL5Rα$^+$ monocytes from blood and lung in the DIO model. $n = 5$ mice per group; Tukey boxplot, two-tailed unpaired Student's *t*-test. (**j**) qRT–PCR of *Csf2* expression in FACS-purified IL5Rα$^+$ cell types from blood and lung in the DIO model. $n = 5$ mice per group; Tukey boxplot, two-tailed unpaired Student's *t*-test. NS, not significant. Box plots represent median and interquartile range while whiskers represent maximum and minimum values excluding outliers. Each symbol represents one mouse.

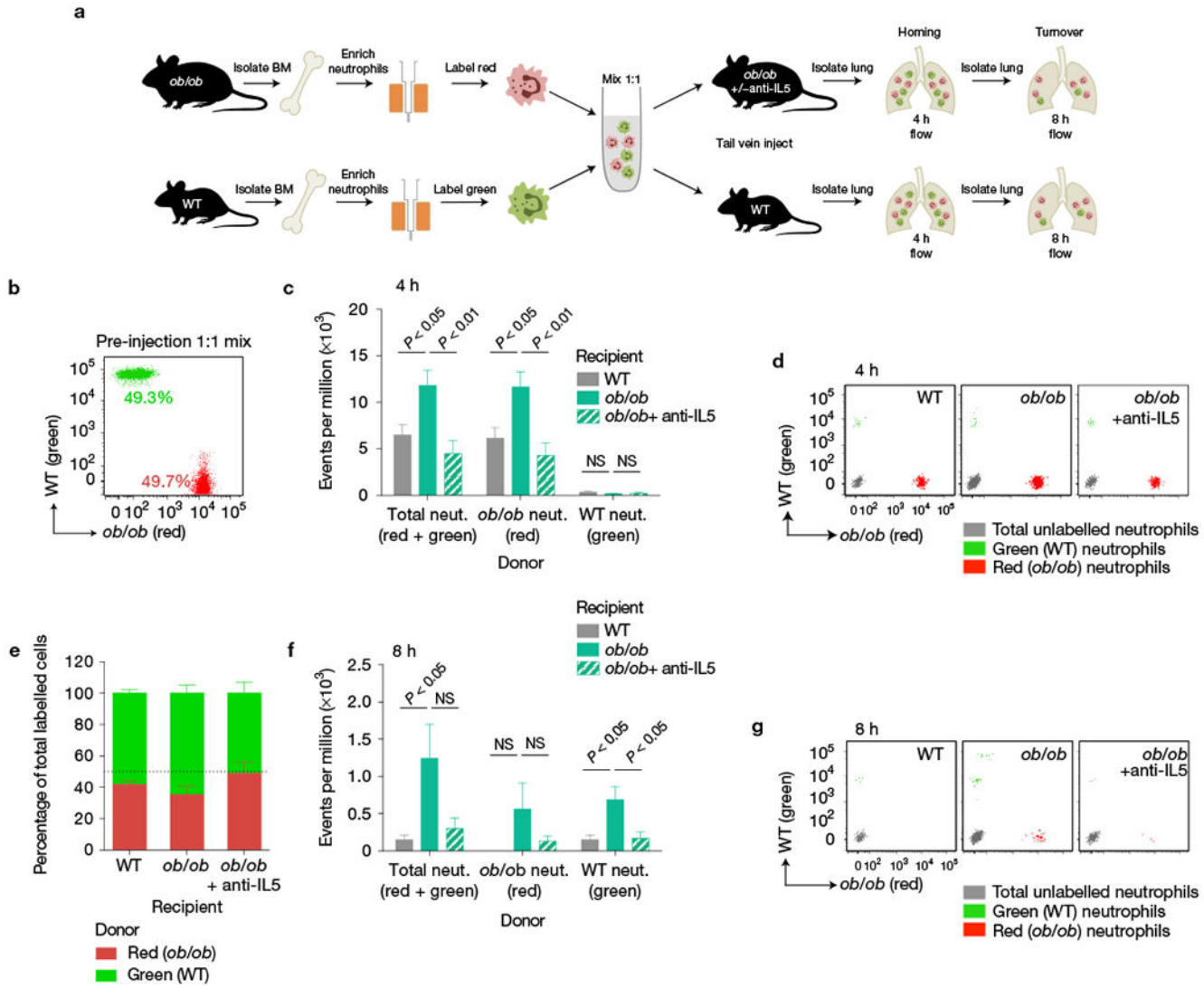

Figure 7.

Obesity enhances lung homing of neutrophils in an IL5-dependent manner. (**a**) Schematic representation of the adoptive cell transfer experiment. Neutrophils were isolated from BM of WT or *ob/ob* mice, labelled with fluorescent CellTrace dye (green and red, respectively), mixed 1:1, and then injected via the tail vein (3×10^6 cells) into WT or *ob/ob* mice ± IL5 neutralizing antibody. Lungs were isolated for flow cytometry analysis after 4 h and 8 h to assess kinetics of neutrophil trafficking. (**b**) Flow cytometry validation of an equal 1:1 mix of WT (green; 49.3%) and *ob/ob* (red; 49.7%) donor neutrophils immediately prior to adoptive cell transfer injections. (**c**) Flow cytometry analysis of lung at 4 h post-adoptive transfer. The vast majority of labelled neutrophils at this time point were from *ob/ob* donors. $n = 5$ mice per recipient group, mean ± s.e.m., one-way ANOVA and Dunnett's multiple comparisons test. (**d**) Representative flow cytometry plots for the data presented in **c**. (**e**) Flow cytometry analysis of fluorescently labelled circulating neutrophils 4 h post-adoptive transfer, demonstrating balanced representation of both red (*ob/ob* donor) and green (WT

donor) cells. $n = 5$ mice per recipient group; mean ± s.e.m. (**f**) Flow cytometry analysis of lung at 8 h post-adoptive transfer. Equivalent representation of red and green donor neutrophils was observed at this time point compared with 4 h as in **c**. $n = 5$ mice per recipient group, mean ± s.e.m., one-way ANOVA and Dunnett's multiple comparisons test. (**g**) Representative flow cytometry plots for the data presented in **f**. NS, not significant.

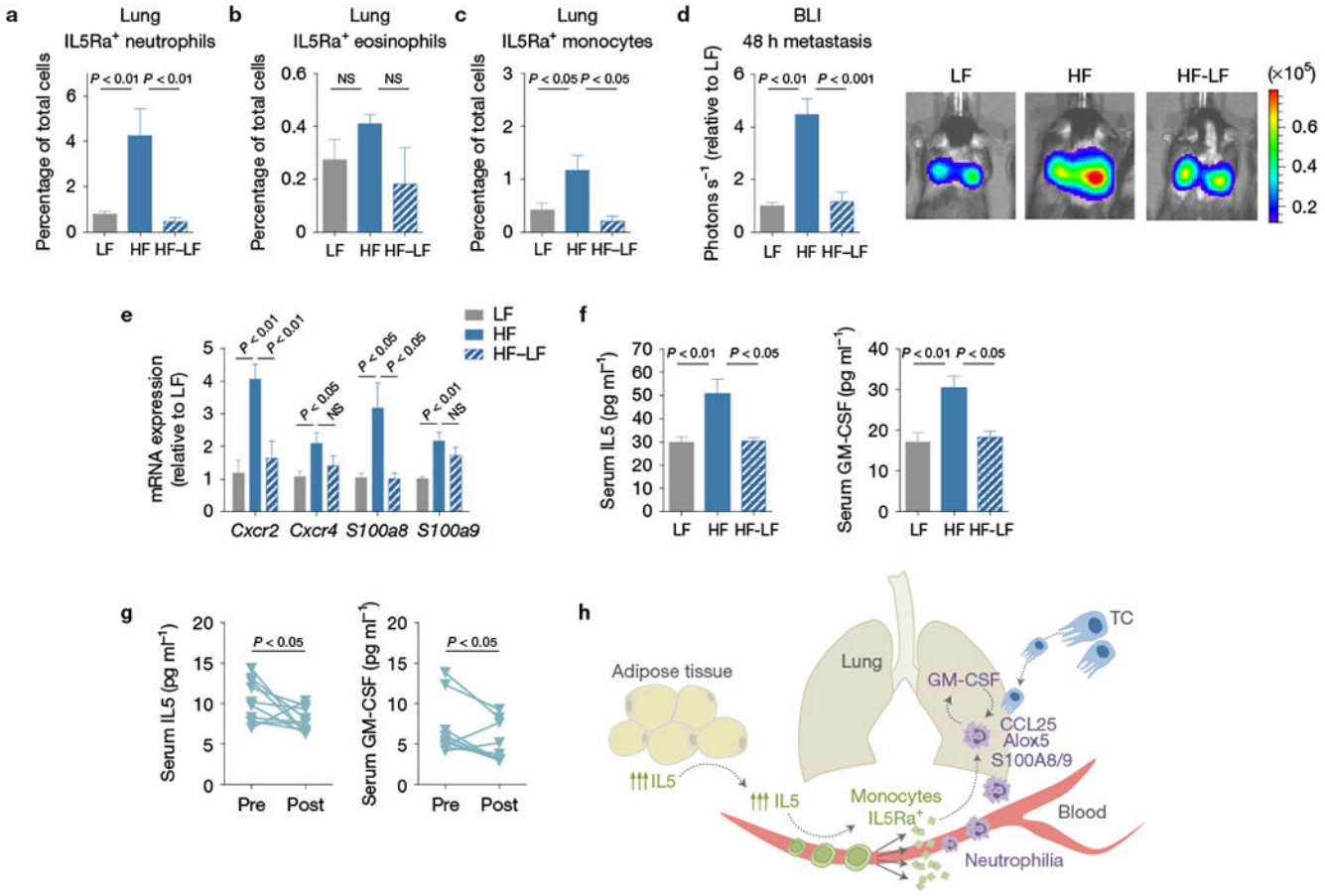

Figure 8.

Weight loss reduces obesity-associated lung neutrophilia and metastasis in mice and humans. (**a**–**c**) Flow cytometry quantification of IL5Rα$^+$ neutrophils (**a**), IL5Rα$^+$ eosinophils (**b**) and IL5Rα$^+$ monocytes (**c**) from lung in LF, HF and diet-switch (HF–LF) mice. LF, $n = 5$ mice; HF, $n = 5$ mice; HF–LF, $n = 4$ mice; mean ± s.e.m., one-way ANOVA and Dunnett's multiple comparisons test. (**d**) Left, BLI of the 48 h metastasis assay with 99LN cells injected via the tail vein in the diet-switch trial. Right, representative images are shown. LF, $n = 9$ mice; HF, $n = 10$ mice; HF–LF, $n = 10$ mice; mean ± s.e.m., Kruskal–Wallis and Dunn's multiple comparisons test. (**e**) qRT-PCR analysis of *Cxcr2, Cxcr4, S100a8* and *S100a9* expression in FACS-purified lung neutrophils. LF, $n = 5$ mice; HF, $n = 5$ mice; HF–LF, $n = 4$ mice; mean ± s.e.m., one-way ANOVA and Dunnett's multiple comparisons test. (**f**) ELISA analysis of serum IL5 (left) and GM-CSF (right). LF, $n = 5$ mice; HF, $n = 5$ mice; HF–LF, $n = 4$ mice; mean ± s.e.m., one-way ANOVA and Dunnett's multiple comparisons test. (**g**) ELISA analysis of serum IL5 (left) and GM-CSF (right) from human weight loss study. $n = 10$ donors per group; matched pre- and post-weight loss concentrations within a given individual are connected with a line; two-tailed paired Student's *t*-test. NS, not significant. (**h**) Schematic representation of the proposed mechanism underlying obesity-associated lung neutrophilia. Adipose tissue-derived IL5 signals to IL5rα$^+$ cells, leading to their expansion and upregulation of *Csf2*. This contributes

to an environment that supports neutrophilia in the circulation and in the lungs. Lung neutrophils are reprogrammed by obesity to adopt pro-tumorigenic transcriptional signatures, and ultimately support metastatic progression.